

<sup>1</sup> **LIGO Detector Characterization in the first half of  
2 the fourth Observing run.**

S. Soni <sup>1</sup>, B. K. Berger <sup>2</sup>, D. Davis<sup>3</sup>, F. Di. Renzo <sup>4</sup>,  
A. Effler <sup>5</sup>, T. A. Ferreira<sup>6</sup>, J. Glanzer <sup>6</sup>, E. Goetz <sup>7</sup>,  
G. González<sup>6</sup>, A. Helmling-Cornell <sup>8</sup>, B. Hughey<sup>9</sup>,  
R. Huxford<sup>10</sup>, B. Mannix<sup>8</sup>, G. Mo<sup>1</sup>, D. Nandi<sup>6</sup>, A. Neunzert<sup>11</sup>,  
S. Nichols<sup>6</sup>, K. Pham <sup>12</sup>, A. I. Renzini<sup>3,13</sup>,  
R. M. S. Schofield<sup>8,11</sup>, A. Stuver <sup>14</sup>, M. Trevor<sup>15</sup>,  
S. Álvarez-López <sup>1</sup>, R. Beda<sup>7</sup>, C. P. L. Berry <sup>14</sup> S. Bhuiyan<sup>7</sup>,  
L. Blagg<sup>8</sup>, R. Bruntz<sup>43</sup>, S. Callos <sup>8</sup>, M. Chan<sup>7</sup>, P. Charlton<sup>39</sup>,  
N. Christensen<sup>41,42</sup>, G. Connolly<sup>8</sup>, R. Dhatri <sup>7</sup>, J. Ding<sup>7</sup>,  
V. Garg<sup>38</sup>, K. Holley-Bockelmann<sup>47,48</sup>, S. Hourihane <sup>10</sup>,  
K. Jani<sup>47</sup>, K. Janssens<sup>40,41</sup>, S. Jarov<sup>7</sup>, A. M. Knee <sup>10</sup>,  
A. Lattal<sup>42</sup>, Y. Lecoeuche <sup>10</sup>, T. Littenberg<sup>44</sup>, A. Liyanage<sup>7</sup>,  
B. Lott<sup>42</sup>, R. Macas<sup>31</sup>, D. Malakar<sup>27</sup>, K. McGowan<sup>47,48</sup>,  
J. McIver<sup>7</sup>, M. Millhouse <sup>10</sup>, L. Nuttall <sup>10</sup>, D. Nykamp<sup>42</sup>,  
I. Ota <sup>10</sup>, C. Rawcliffe<sup>37</sup>, B. Scully<sup>7</sup>, J. Tasson<sup>42</sup>, A. Tejera <sup>10</sup>,  
S. Thiele<sup>7</sup>, R. Udall<sup>3</sup>, C. Winborn<sup>27</sup>, Z. Yarbrough<sup>6</sup>, Z. Zhang<sup>42</sup>,  
Y. Zheng<sup>27</sup>, R. Abbott<sup>3</sup>, I. Abouelfettouh<sup>11</sup>, R. X. Adhikari <sup>10</sup>,  
A. Ananyeva<sup>3</sup>, S. Appert<sup>3</sup>, K. Arai <sup>10</sup>, N. Aritomi<sup>11</sup>,  
S. M. Aston<sup>5</sup>, M. Ball <sup>10</sup>, S. W. Ballmer<sup>16</sup>, D. Barker<sup>11</sup>,  
L. Barsotti <sup>10</sup>, J. Betzwieser <sup>10</sup>, G. Billingsley <sup>10</sup>, S. Biscans<sup>1,6</sup>,  
N. Bode <sup>10</sup>, E. Bonilla <sup>10</sup>, V. Bossilkov<sup>5</sup>, A. Branch<sup>5</sup>,  
A. F. Brooks <sup>10</sup>, D. D. Brown<sup>19</sup>, J. Bryant<sup>20</sup>, C. Cahillane <sup>10</sup>,  
H. Cao<sup>21</sup>, E. Capote<sup>16</sup>, F. Clara<sup>11</sup>, J. Collins<sup>5</sup>,  
C. M. Compton<sup>11</sup>, R. Cottingham<sup>5</sup>, D. C. Coyne <sup>10</sup>,  
R. Crouch<sup>11</sup>, J. Csizmazia<sup>11</sup>, T. J. Cullen<sup>3</sup>, L. P. Dartez<sup>11</sup>,  
N. Demos<sup>1</sup>, E. Dohmen<sup>11</sup>, J. C. Driggers <sup>10</sup>, S. E. Dwyer<sup>11</sup>,  
A. Ejlli <sup>10</sup>, T. Etzel<sup>3</sup>, M. Evans <sup>10</sup>, J. Feicht<sup>3</sup>, R. Frey <sup>10</sup>,  
W. Frischhertz<sup>5</sup>, P. Fritschel<sup>1</sup>, V. V. Frolov<sup>5</sup>, P. Fulda<sup>23</sup>,  
M. Fyffe<sup>5</sup>, D. Ganapathy <sup>10</sup>, B. Gateley<sup>11</sup>, J. A. Giaime <sup>10</sup>,  
K. D. Giardina<sup>5</sup>, R. Goetz <sup>10</sup>, A. W. Goodwin-Jones <sup>10</sup>,  
S. Gras<sup>1</sup>, C. Gray<sup>11</sup>, D. Griffith<sup>3</sup>, H. Grote <sup>10</sup>, T. Guidry<sup>11</sup>,  
E. D. Hall <sup>10</sup>, J. Hanks<sup>11</sup>, J. Hanson<sup>5</sup>, M. C. Heintze<sup>5</sup>,  
N. A. Holland <sup>10</sup>, D. Hoyland<sup>20</sup>, H. Y. Huang <sup>10</sup>, Y. Inoue<sup>26</sup>,  
A. L. James <sup>10</sup>, A. Jennings<sup>11</sup>, W. Jia<sup>1</sup>, S. Karat<sup>3</sup>, S. Karki <sup>10</sup>,  
M. Kasprzack <sup>10</sup>, K. Kawabe<sup>11</sup>, N. Kijbunchoo <sup>10</sup>, P. J. King<sup>11</sup>,

38 J. S. Kissel <sup>11</sup>, K. Komori<sup>1</sup>, A. Kontos <sup>28</sup>, R. Kumar<sup>11</sup>,  
 39 K. Kuns <sup>1</sup>, M. Landry<sup>11</sup>, B. Lantz <sup>2</sup>, M. Laxen <sup>5</sup>, K. Lee <sup>29</sup>,  
 40 M. Lesovsky<sup>3</sup>, F. Llamas<sup>30</sup>, M. Lormand<sup>5</sup>, H. A. Loughlin<sup>1</sup>,  
 41 M. MacInnis<sup>1</sup>, C. N. Makarem<sup>3</sup>, G. L. Mansell <sup>16,1</sup> ,  
 42 R. M. Martin <sup>32</sup> , K. Mason<sup>1</sup> , F. Matichard<sup>3</sup> ,  
 43 N. Mavalvala <sup>1</sup>, N. Maxwell<sup>11</sup>, G. McCarrol<sup>5</sup>, R. McCarthy<sup>11</sup>,  
 44 D. E. McClelland <sup>33</sup>, S. McCormick<sup>5</sup>, L. McCuller <sup>3</sup>,  
 45 T. McRae<sup>33</sup>, F. Mera<sup>11</sup>, E. L. Merilh<sup>5</sup>, F. Meylahn <sup>17,18</sup>,  
 46 R. Mittleman<sup>1</sup>, D. Moraru<sup>11</sup>, G. Moreno<sup>11</sup>, A. Mullavey<sup>5</sup>,  
 47 M. Nakano<sup>5</sup>, T. J. N. Nelson<sup>5</sup>, J. Notte<sup>32</sup>, J. Oberling<sup>11</sup>,  
 48 T. O'Hanlon<sup>5</sup>, C. Ostheder<sup>3</sup>, D. J. Ottaway <sup>19</sup>, H. Overmier<sup>5</sup>,  
 49 W. Parker <sup>5</sup>, A. Pele <sup>3</sup>, H. Pham<sup>5</sup>, M. Pirello<sup>11</sup>,  
 50 V. Quetschke<sup>30</sup>, K. E. Ramirez <sup>5</sup>, J. Reyes<sup>32</sup>,  
 51 J. W. Richardson <sup>21</sup>, M. Robinson<sup>11</sup>, J. G. Rollins <sup>3</sup>,  
 52 C. L. Romel<sup>11</sup>, J. H. Romie<sup>5</sup>, M. P. Ross <sup>34</sup>, K. Ryan<sup>11</sup>,  
 53 T. Sadecki<sup>11</sup>, A. Sanchez<sup>11</sup>, E. J. Sanchez<sup>3</sup>, L. E. Sanchez<sup>3</sup>,  
 54 R. L. Savage <sup>11</sup>, D. Schaetzl<sup>3</sup>, M. G. Schiworski <sup>19</sup>,  
 55 R. Schnabel <sup>35</sup>, E. Schwartz <sup>22</sup>, D. Sellers<sup>5</sup>, T. Shaffer<sup>11</sup>,  
 56 R. W. Short<sup>11</sup>, D. Sigg <sup>11</sup>, B. J. J. Slagmolen <sup>33</sup>, C. Soike<sup>11</sup>,  
 57 V. Srivastava<sup>16</sup>, L. Sun <sup>33</sup>, D. B. Tanner<sup>23</sup>, M. Thomas<sup>5</sup>,  
 58 P. Thomas<sup>11</sup>, K. A. Thorne<sup>5</sup>, C. I. Torrie<sup>3</sup>, G. Traylor<sup>5</sup>,  
 59 A. S. Ubhi<sup>20</sup>, G. Vajente <sup>3</sup>, J. Vanosky<sup>3</sup>, A. Vecchio <sup>20</sup>,  
 60 P. J. Veitch <sup>19</sup>, A. M. Vibhute <sup>11</sup>, E. R. G. von Reis<sup>11</sup>,  
 61 J. Warner<sup>11</sup>, B. Weaver<sup>11</sup>, R. Weiss<sup>1</sup>, C. Whittle <sup>1</sup>,  
 62 B. Willke <sup>18,17,18</sup>, C. C. Wipf<sup>3</sup>, V. A. Xu <sup>1</sup>, H. Yamamoto <sup>3</sup>,  
 63 L. Zhang<sup>3</sup>, M. E. Zucker<sup>1,3</sup>

64 <sup>1</sup>LIGO, Massachusetts Institute of Technology, Cambridge, MA 02139, USA  
 65 <sup>2</sup>Stanford University, Stanford, CA 94305, USA

66 <sup>3</sup>LIGO, California Institute of Technology, Pasadena, CA 91125, USA  
 67 <sup>4</sup>Université Lyon, Université Claude Bernard Lyon 1, CNRS, IP2I Lyon IN2P3, UMR  
 68 5822, F-69622 Villeurbanne, France

69 <sup>5</sup>LIGO Livingston Observatory, Livingston, LA 70754, USA  
 70 <sup>6</sup>Louisiana State University, Baton Rouge, LA 70803, USA

71 <sup>7</sup>University of British Columbia, Vancouver, BC V6T 1Z4, Canada  
 72 <sup>8</sup>University of Oregon, Eugene, OR 97403, USA

73 <sup>9</sup>Embry-Riddle Aeronautical University, Prescott, AZ 86301, USA  
 74 <sup>10</sup>The Pennsylvania State University, University Park, PA 16802, USA

75 <sup>11</sup>LIGO Hanford Observatory, Richland, WA 99352, USA  
 76 <sup>12</sup>School of Physics and Astronomy, University of Minnesota, 55455 MN, USA  
 77 <sup>13</sup>Dipartimento di Fisica “G. Occhialini”, Università degli Studi di Milano-Bicocca,  
 78 Piazza della Scienza 3, 20126 Milano, Italy

79 <sup>14</sup>Villanova University, 800 Lancaster Ave, Villanova, PA 19085, USA  
 80 <sup>15</sup>University of Maryland, College Park, MD 20742, USA

81 <sup>16</sup>Syracuse University, Syracuse, NY 13244, USA

82                   <sup>17</sup>Max Planck Institute for Gravitational Physics (Albert Einstein Institute),  
83                   D-30167 Hannover, Germany  
84                   <sup>18</sup>Leibniz Universität Hannover, D-30167 Hannover, Germany  
85                   <sup>19</sup>OzGrav, University of Adelaide, Adelaide, South Australia 5005, Australia  
86                   <sup>20</sup>University of Birmingham, Birmingham B15 2TT, United Kingdom  
87                   <sup>21</sup>University of California, Riverside, Riverside, CA 92521, USA  
88                   <sup>22</sup>Cardiff University, Cardiff CF24 3AA, United Kingdom  
89                   <sup>23</sup>University of Florida, Gainesville, FL 32611, USA  
90                   <sup>24</sup>OzGrav, University of Western Australia, Crawley, Western Australia 6009,  
91                   Australia  
92                   <sup>25</sup>Vrije Universiteit Amsterdam, 1081 HV, Amsterdam, Netherlands  
93                   <sup>26</sup>National Central University, Taoyuan City 320317, Taiwan  
94                   <sup>27</sup>Missouri University of Science and Technology, Rolla, MO 65409, USA  
95                   <sup>28</sup>Bard College, Annandale-On-Hudson, NY 12504, USA  
96                   <sup>29</sup>Sungkyunkwan University, Seoul 03063, Republic of Korea  
97                   <sup>30</sup>The University of Texas Rio Grande Valley, Brownsville, TX 78520, USA  
98                   <sup>31</sup>Institute of Cosmology and Gravitation, University of Portsmouth, Portsmouth,  
99                   PO1 3FX, UK  
100                  <sup>32</sup>Montclair State University, Montclair, NJ 07043, USA  
101                  <sup>33</sup>OzGrav, Australian National University, Canberra, Australian Capital Territory  
102                  0200, Australia  
103                  <sup>34</sup>University of Washington, Seattle, WA 98195, USA  
104                  <sup>35</sup>Universität Hamburg, D-22761 Hamburg, Germany  
105                  <sup>36</sup>Oberlin College, Oberlin, OH 44074, USA.  
106                  <sup>37</sup>Durham University, South Road, Durham, ,DH1 3LE, UK  
107                  <sup>38</sup>University College London, Gower St, London WC1E 6BT, United Kingdom  
108                  <sup>39</sup>OzGrav, Charles Sturt University, Wagga Wagga, New South Wales 2678, Australia  
109                  <sup>40</sup>Universiteit Antwerpen, Prinsstraat 13, 2000 Antwerpen, Belgium  
110                  <sup>41</sup>Université Côte d'Azur, Observatoire de la Côte d'Azur, CNRS, Artemis, 06304  
111                  Nice, France  
112                  <sup>42</sup>Carleton College, Northfield, MN 55057, USA  
113                  <sup>43</sup>Christopher Newport University, Newport News, VA 23606, USA  
114                  <sup>44</sup>NASA Marshall Space Flight Center, Huntsville, Alabama 35811, USA  
115                  <sup>45</sup>School of Physics, Georgia Institute of Technology, Atlanta, Georgia 30332, USA  
116                  <sup>46</sup>SUPA, School of Physics and Astronomy, University of Glasgow, University Ave,  
117                  Glasgow G12 8QQ, United Kingdom  
118                  <sup>47</sup>Vanderbilt University, Department of Physics and Astronomy, 6301 Stevenson  
119                  Science Center, Nashville, TN 37212, USA  
120                  <sup>48</sup>Fisk University, Department of Life and Physical Sciences, 1000 17th Avenue N.  
121                  Nashville, TN 37208, USA  
122                  E-mail: siddharthsoni22@gmail.com

123                  **Abstract.** Progress in gravitational-wave astronomy depends upon having sensitive  
124                  detectors with good data quality. Since the end of the LIGO-Virgo-KAGRA third  
125                  Observing run in March 2020, detector-characterization efforts have lead to increased  
126                  sensitivity of the detectors, swifter validation of gravitational-wave candidates and  
127                  improved tools used for data-quality products. In this article, we discuss these efforts  
128                  in detail and their impact on our ability to detect and study gravitational-waves. These  
129                  include the multiple instrumental investigations that led to reduction in transient noise,  
130                  along with the work to improve software tools used to examine the detectors data-  
131                  quality. We end with a brief discussion on the role and requirements of detector

characterization as the sensitivity of our detectors further improves in the future Observing runs.

## 1. Introduction

The Laser Interferometer Gravitational-Wave Observatory (LIGO) [1] and Virgo [2] detectors started the era of gravitational-wave (GW) astronomy when the first GW signal from the merger of two black holes was detected in 2015 [3]. Since then, the LIGO, Virgo and KAGRA collaborations have published 90 probable detections of signals involving black holes and neutron stars, including the spectacular multi-messenger discovery in August 2017 [4–7]. The data used for these analyses is publicly available in the Gravitational Wave Open Science Center (GWOSC) ‡. The LIGO and KAGRA detectors started taking data in the fourth observing run (O4) on May 24, 2023. The first part of the run, O4a, finished on January 16, 2024. The LIGO and Virgo detectors started taking data again on April 10, 2024 (O4b). In O4a, 92 significant detection candidates were shared as public alerts, including 11 retracted for data-quality problems. The 81 significant detections are almost as many as the 90 detections published in the GWTC-3 catalog [6] from the previous three Observing runs.

As shown in figure 1, the broadband sensitivity of the LIGO detectors in O4a was significantly better than in O3b. Some key upgrades commissioned between third observing run (O3) and O4 include frequency-dependent squeezing [8], replacement of some optics that had small defects (point absorbers) allowing for increased laser power, and replacing squeezing subsystem Faraday isolators with more efficient ones to increase the level of squeezing achieved [9]. As a measure of sensitivity, we can calculate the distance to which the noise would allow a detection of a binary neutron star (BNS) system ( $1.4 M_{\odot}$  each) with a signal-to-noise ratio of 8; this is often called the “binary neutron star inspiral range” or “BNS range”. The spectra shown in figure 1 correspond to dates in O3b (LIGO Hanford (LHO) March 19, 2020, and LIGO Livingston (LLO) January 4, 2020) with BNS ranges 112 Mpc and 134 Mpc respectively; and dates in O4a (LHO December 12 2023, and LLODecember 31 2023) with BNS ranges 160 Mpc and 158 Mpc respectively.

At the junction between instrument scientists and data analysis groups, the Detector Characterization (DetChar) group works to understand instrumental noise and improve data-quality [10]. The group carries out instrumental investigations in collaboration with instrument scientists at the observatory sites, striving to understand and mitigate sources of noise that are not inherent to the detector design and thereby to improve detector performance. The DetChar group also provides data-quality information for GW searches, which is crucial to avoid or remove noise artifacts, and to evaluate and validate gravitational-wave signals.

‡ [www.gwosc.org](http://www.gwosc.org)

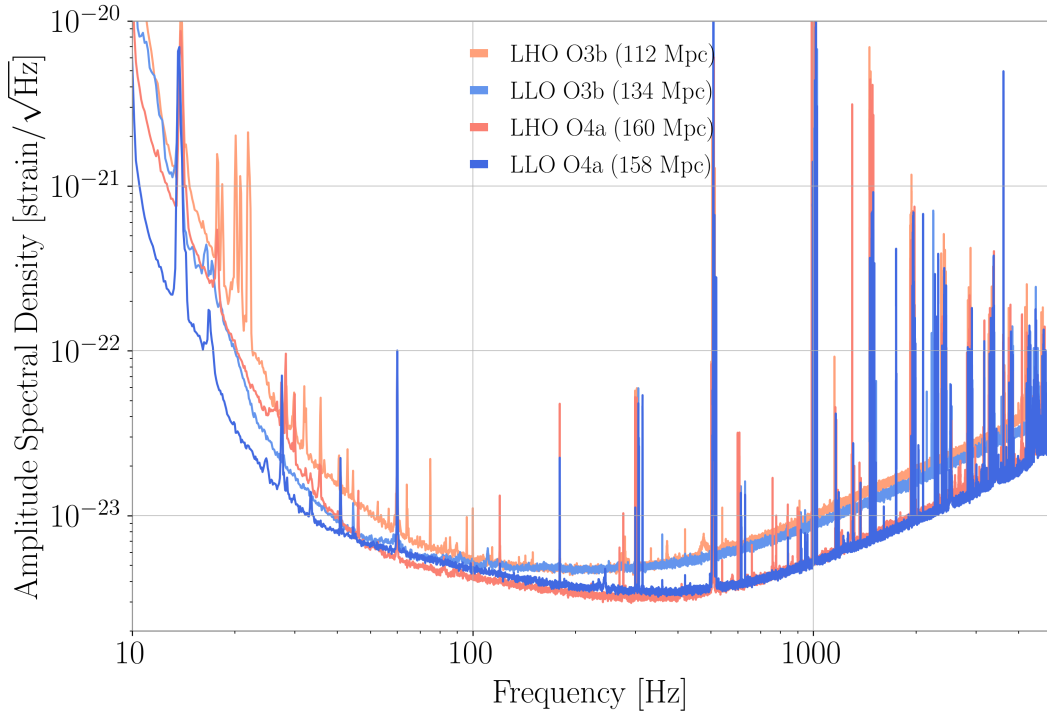


Figure 1: Typical amplitude spectral densities of strain noise at LHO and LLO detectors in O3b and O4a. The notable improvement in broadband noise reduction observed in O4a is due to various factors including the reduction of scattered-light noise, commissioning of feedback control loops, and the implementation of frequency-dependent squeezing. At LLO, the strain noise near 100 Hz is slightly higher than at LHO, possibly due to higher thermal noise in end test masses replaced at LLO. At low frequencies, the strain noise in both detectors was significantly improved with the removal of a septum window that was coupling ground vibration through scattered light. The damping of baffle resonances also reduced the coupling of scattered light. At LHO, an alignment dither system that was used in O3 and produced narrow features around 20 Hz was replaced by a camera servo to avoid the appearance of those lines.

The DetChar group carries out a variety of regular activities to monitor noise and provide data-quality information to searches. The LIGO DetChar summary pages [11] provide detector-site and off-site scientists, technicians, and staff an overview of the performance of the LIGO detectors and environmental monitors through a series of regularly updated webpages. Apart from the primary gravitational wave channel that records the strain, there are thousands of auxiliary channels monitoring the state of environment and various detector components. The summary pages centralize plots, figures of merit, and links to additional resources for analyses of the GW strain data and various detector subsystems and auxiliary channels. During Observing runs, members of the DetChar group participate in data-quality shifts, which utilize the summary

179 pages to closely monitor the performance of the detector. Members also engage in event  
180 validation shifts in order to assess any data-quality issues near and during the time of  
181 GW signals [12]. Finally, the DetChar group works together with GW analysis efforts to  
182 construct data-quality products in order to avoid noise contamination in GW analyses  
183 (see section 4.)

184 Data recorded by the LIGO detectors can be characterized as generally Gaussian  
185 and stationary with non-Gaussian noise appearing in several forms: 1) short-duration  
186 artifacts, often referred to as “glitches”, which are typically broadband in nature; 2)  
187 persistent or slowly time-varying, broadband artifacts; 3) persistent or slowly time-  
188 varying, narrowband artifacts, often referred to as “lines” [13]. Typically, glitches  
189 impact transient GW searches and parameter estimation of candidate transient GW  
190 events but do not strongly impact searches for persistent GW. Similarly, lines impact  
191 persistent GW searches but do not strongly impact searches and parameter estimation  
192 for transient GW. Persistent broadband artifacts impact all types of searches because  
193 the artifacts elevate the noise background.

194 Glitches and lines can be further categorized by the morphology of the artifact.  
195 Many common glitch classes have been named (e.g., Tomte, Fast Scattering, Low  
196 Frequency Burst) based on a combination of their shape in spectrogram plots and what  
197 is known of their origin, see figure 2 [14, 15]. Some glitch classes are more detrimental to  
198 transient gravitational-wave searches and compact binary coalescence (CBC) parameter  
199 estimation than others. Lines, by contrast, have fewer morphological distinctions,  
200 see figure 3 [16]. The primary distinction is between individual line artifacts and combs  
201 of lines. Combs arise when narrowband noise that couples into the gravitational-wave  
202 data is not purely sinusoidal, creating a series of spectral peaks with common frequency  
203 spacing. Combs are particularly problematic because one source can impact multiple  
204 narrow frequency bands at the same time.

205 This paper describes the activities performed to characterize the strain data  
206 measured by the LIGO detectors, and investigations of instrumental and environmental  
207 noise between the end of O3 and end of O4a. In section 2, we describe the instrumental  
208 investigations. In section 3 we describe the activities to promptly validate gravitational-  
209 wave candidates, using tools to analyze the data-quality surrounding the event. In  
210 section 4, we describe the use of data-quality products in searches of gravitational-waves  
211 of different kinds (compact binary coalescences, un-modelled transients, continuous  
212 waves and stochastic background). In section 5, we summarize the results, draw  
213 conclusions and present prospects for the near future.

## 214 2. Instrumental Investigations

215 Instrumental investigations carried out by the DetChar group are crucial for  
216 understanding the impact of various noise sources on detector data quality [19]. The  
217 Physical Environment and Monitoring (PEM) investigations are often carried out at the  
218 sites and require a strong co-ordination between the DetChar group and the instrument

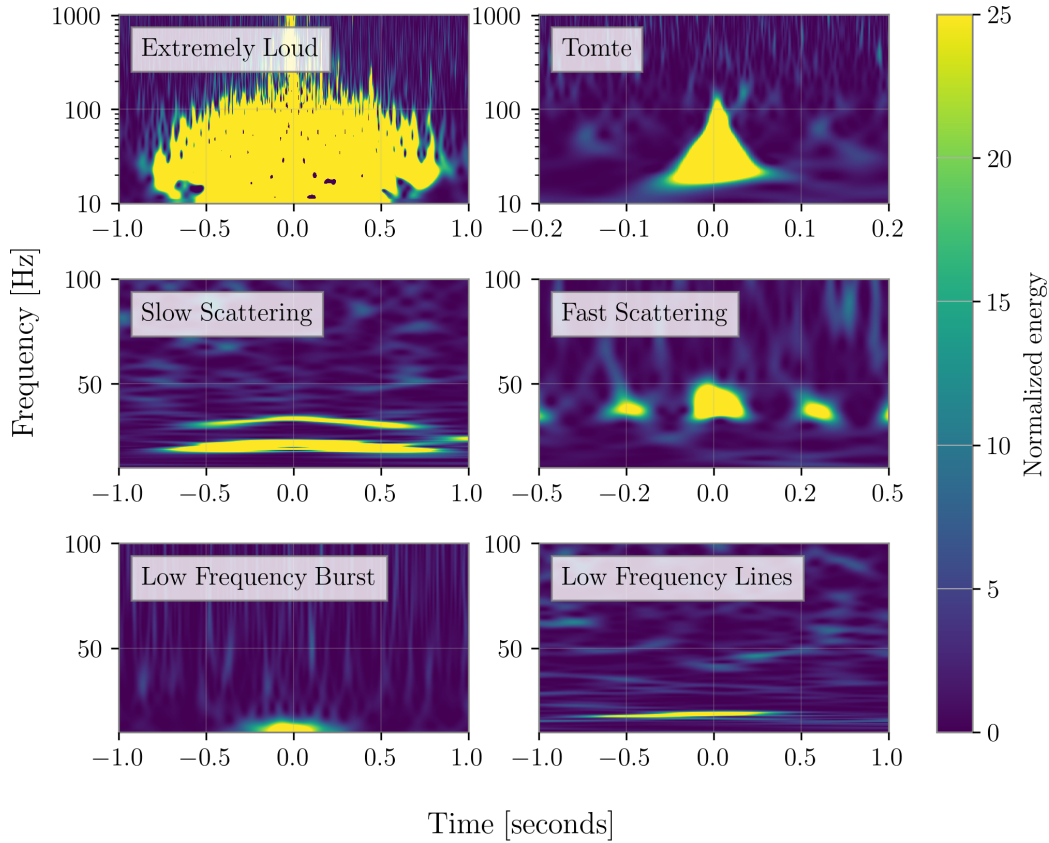


Figure 2: Time-frequency spectrograms of glitches that are common at either LHO or LLO. For Extremely Loud and Tomte, we have not yet found any source. Slow Scattering and Fast Scattering show a strong coupling with increased ground motion and are caused by light scattering [17, 18]. O4a has seen an increased rate of Low Frequency Burst and Low Frequency Lines at both detectors for which we have not identified a source yet.

219 scientists [20]. These investigations rely on vibration, acoustic, and magnetic injections,  
 220 which enable us to estimate environmental couplings between different parts of the  
 221 detector and the GW strain data. As explained in detail later in this section, some noise  
 222 couplings can be reduced or eliminated, thereby reducing the amount of noise in GW  
 223 strain channel. In addition to artificially inducing environmental noise, we also routinely  
 224 induce differential-arm displacements via the photon calibrators [21] to study coupling  
 225 between the GW channel and interferometer auxiliary channels (see section 2.1.4) and  
 226 add simulated gravitational waveforms for end-to-end testing of analysis pipelines [22].

227 In addition to artificially induced environmental noise and signals studies,  
 228 the DetChar group also analyzes instrument data in other ways to enhance our  
 229 understanding of the detector. These studies usually use several DetChar tools for  
 230 determining the coupling between the environment, auxiliary sensors, and the detector  
 231 noise characteristics. For example, through these investigations we may find that ground

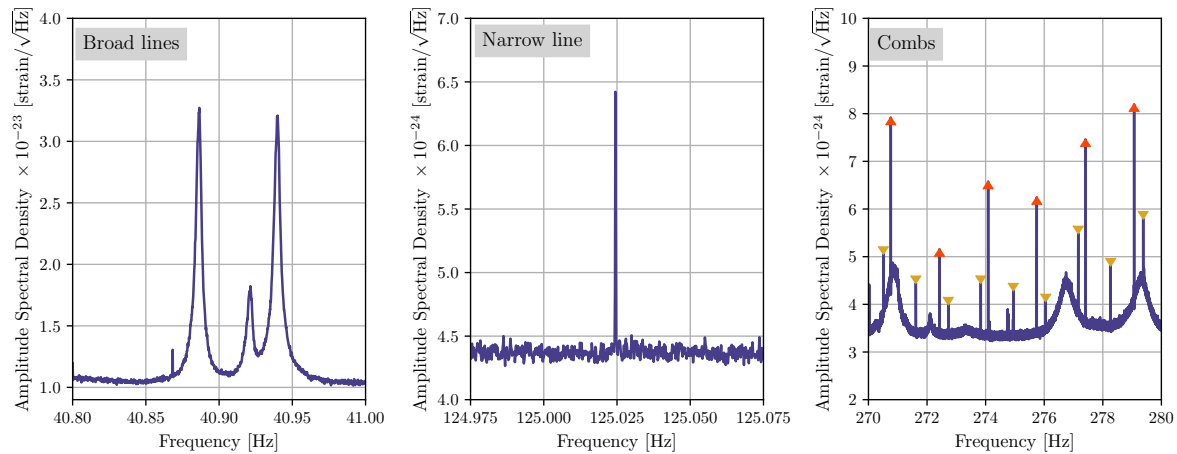


Figure 3: Amplitude spectral density plots of LHO strain data showing common line artifact classes that occur at both detectors in high-resolution spectra ( $\Delta f = 1/1800$  Hz). Left panel: an example of persistent broad noise artifact arising from interferometer mirror suspension roll-mode resonances. Middle panel: an example of a narrow line of unknown origin. Right panel: an example of two combs (as well as some broader noise artifacts) where upright and inverted triangles mark the two combs with distinct spacing in frequency.

232 motion at a specific location in the detector is more correlated to the noise in the GW  
233 strain channel than at other locations. Such hypothesis can then be tested using the  
234 PEM tests.

235 These investigations are central to solving problems that adversely impact the  
236 detector data-quality and uptime, consequently reducing the number of gravitational-  
237 wave observations. The transient noise impacts the parameter estimation process and  
238 could generate false alerts, which have to be retracted later. In this section, we first  
239 give an overview of transient noise in O4a at both the detectors, and then we discuss  
240 several DetChar investigations carried out between the end of O3 and the end of O4a.

### 241 2.1. Transient noise investigations at both sites

242 2.1.1. *Transient Noise* Glitches are short-duration bursts of excess power with their  
243 origins in environmental and/or instrumental couplings. Omicron is an event trigger  
244 generator used to search for this excess power in the primary gravitational channel,  
245  $h(t)$ , and auxiliary channels [23]. The time, frequency, and signal-to-noise ratio (SNR)  
246 of short-duration transient noise can be visualized using “glitchgrams”. Figure 4 shows  
247 an example of a glitchgram which is generated by plotting Omicron triggers.

248 Different tools are used to investigate glitches, and one of them is Gravity Spy,  
249 which classifies noise transients by their morphologies in spectrograms [14, 15, 24, 25].  
250 Figure 2 shows time-frequency spectrograms for six common glitch categories at the two  
251 sites [26, 27]. Certain environmental or instrumental conditions can generate similar

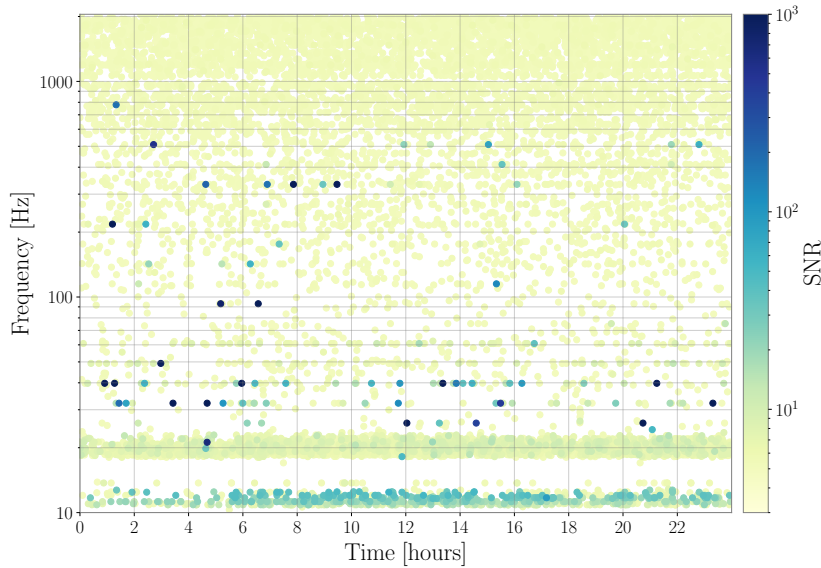


Figure 4: A glitchgram of Omicron triggers produced using LLO data for one day during O4a; with its peak frequency plotted on the vertical axis and its SNR indicated by the color.

signals. Glitch classification enables the identification of patterns in the data for similar noise transients.

Examining the relationship between noise in the primary gravitational-wave channel ( $h(t)$ ) and multiple auxiliary channels can potentially lead us to the source of the noise. Hveto is one of the main tools used to study the correlation between transient noise in the primary strain and auxiliary data [28]. Auxiliary channels that also witness the same noise are called witness channels. The glitchgram shown in figure 4 is from a day when seismometers recorded elevated ground motion, which caused the excess transient noise at low frequencies around 10–20 Hz. Sometimes, this motion is so strong that the interferometer cannot maintain the servo-controlled resonance condition and stops observing [29]. This is referred to as losing lock of the interferometer.

Multiple variables affect the glitch rate in the detectors, including instrumental upgrades, addition of new detector components, and environmental conditions such as wind, elevated ground motion, or the passing of trucks or trains near the site. Figure 5 shows the comparison of glitch rates between O3 and O4 for two different SNR thresholds. In O3, transient noise at both detectors was dominated by stray light. These couplings were greatly reduced during O3b and after O3. Further details are discussed in [17, 18] and in section 2.3.

The O4a transient noise at LHO was dominated by low SNR glitches mostly in 10–50 Hz. Most of the LHO transient noise was low SNR as can be seen in figure 5 and in figure 6, which shows the daily glitch rate at LHO and LLO during O4a. These broadband transients had a common source and were mitigated during O4a. Section 2.2.2 provides more details on this.

The transient noise at LLO was dominated by low-frequency ground motion that induce laser light scattering. Most of this ground motion can be attributed to the impact of atmosphere driven ocean waves on the ocean surface, also known as microseism [30]. The microseismic motion is seasonal and is caused by intense ocean wave activity from winter storms. This is why we see an increase in the glitch rate during the latter half of O4a as shown in figure 6. Section 2.3.1 provides more detail on this noise.

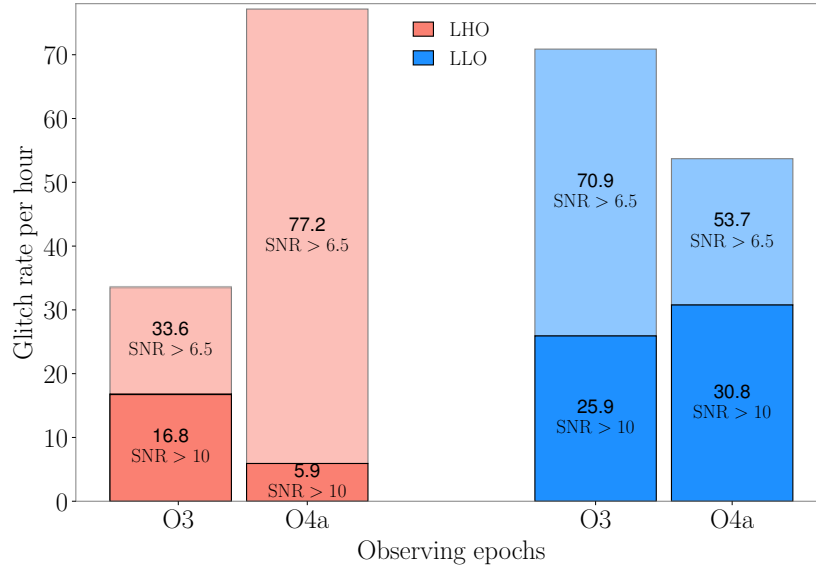


Figure 5: Glitch rates from Omicron during O3 and O4a at LLO and LHO in the frequency band 10–2048 Hz. For each observatory, two distinct rates were calculated: with SNR above 6.5 and with SNR above 10.

*2.1.2. Overview of scattering noise* Noise due to light scattering is a common problem at both detectors. Scattering happens when a small fraction of laser light gets reflected off some optics, hits another moving surface, and then rejoins the main laser beam. This rejoining leads to the introduction of a time-dependent phase modulation to the main laser beam [31]. The additional phase noise shows up as  $h_{\text{ph}}(f)$ ,

$$h_{\text{ph}}(f) = \frac{K}{2} \frac{\lambda}{4\pi L} \mathcal{F}[\sin \delta\phi_{sc}(t)] \quad (1)$$

where

$$\phi(t) = \phi_0 + \delta\phi_{sc}(t) = \frac{4\pi}{\lambda} [x_0 + \delta x_{sc}(t)]. \quad (2)$$

Here,  $K$  is the ratio of stray light amplitude to the amplitude of light in the main beam (usually unknown but small, of the order of  $10^{-9}$  in O4a microseismic scatter),  $\mathcal{F}$  indicates a Fourier transform,  $\lambda$  is laser wavelength (1064 nm) and  $L$  is the length of interferometer arms (4 km),  $x_0$  represents the static path length,  $\delta x_{sc}(t)$  is the time-dependent motion of the scattering surface, which results into additional phase  $\delta\phi_{sc}(t)$  on

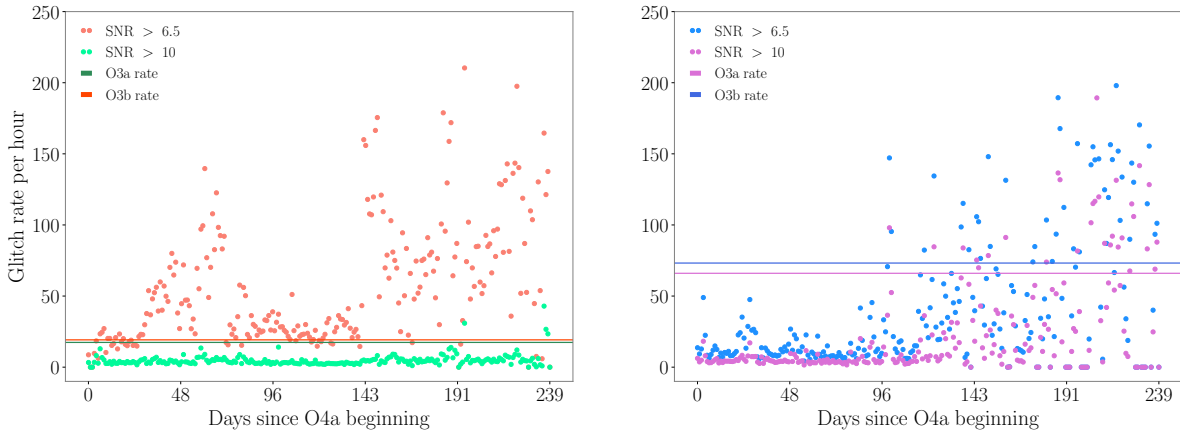


Figure 6: Omicron trigger rate during the O4a at LHO (left panel) and LLO (right panel) in the frequency band 10–2048 Hz. At LHO, most of the glitches had  $\text{SNR} < 10$ . At LLO, there is a visible increase in the rate of transients around the start of October 2023. This is due to unidentified stray light coupling induced by the seasonal increase in the microseismic ground motion.

294 top of the static phase  $\phi_0$  [17, 32–34]. When the relative motion between the scattering  
295 surfaces is not small compared to the laser wavelength, we get fringe wrapping and  
296 the noise shows up as arches in time-frequency spectrograms (see figure 2). Transient  
297 scattering noise can be classified into two categories, which depends on the frequency of  
298 the ground motion that produces it: Slow Scattering and Fast Scattering [17]. Scattering  
299 is discussed in the following section, and again in section 2.3.

300 2.1.3. *Cryo-manifold baffle noise* Most of the optics in LIGO are housed in corner  
301 and end stations (X-arm and Y-arm). During O3, vibrating cryo-manifold baffles (CBs)  
302 at the LIGO end stations were identified as a cause of light scattering noise [18, 35].  
303 These baffles prevent most light reflecting from the beamtube reduction flange, where  
304 the beamtube narrows at the corner and end stations, from reentering the detector  
305 arms [36]. Some light reflected from these baffles, however, still interferes with the  
306 circulating light in the main beam. When a mechanical resonance of the CB with a  
307 high quality factor was rung up from heightened ground motion, scattered light noise  
308 at about 4 Hz and harmonics were visible in  $h(t)$ .

309 At both detectors, rubber viton dampers were installed on three of the four CBs  
310 to decrease the quality factor of the mechanical resonance prior to the start of O4a.  
311 Dampers were not installed on the final cryo-manifold baffle (CB) because no other in-  
312 vacuum maintenance work took place in its vicinity during the O3–O4a break. Damping  
313 reduced the velocity of the reflecting surface and thus lowered the cutoff frequency of  
314 the scattering noise to low frequencies where the interferometer is not sensitive. The  
315 vibration coupling at the remaining undamped cryobaffles increased between O3 and  
316 O4 as the power in the arms increased. The difference in coupling between 60 W and

317 75 W input power at the undamped CBs was about a factor of about 3 at LHO [37].

318 In the O4a-O4b commissioning break an incursion was made into each detector's  
319 X-arm end station vacuum enclosure to damp the final cryo-manifold baffle [38]. After  
320 the viton damper installation, the quality factor of the  $\sim$ 4 Hz mechanical mode in the  
321 CB dropped by a factor of  $\sim$ 20, reducing the maximum frequency of the scattering noise  
322 by roughly the same amount [39].

323 *2.1.4. Safety studies* A crucial aspect of verifying gravitational-wave candidates is  
324 ensuring that they are not introduced by environmental noise sources observed in  
325 auxiliary channels. In general, however, the transfer functions between  $h(t)$  (GW strain)  
326 channel and the thousands of auxiliary channels is unknown, so it is possible for real  
327 gravitational-wave events to produce signals in some of the auxiliary channels. If we  
328 were to use such a channel (an “unsafe” channel) to veto a gravitational-wave event,  
329 without knowledge of this coupling, we would in effect be using an astrophysical signal to  
330 veto itself. To probe the “safety” of auxiliary channels for vetoing candidate events, we  
331 use the photon calibrators to inject sine-Gaussian waveforms into  $h(t)$  at each detector,  
332 mimicking a gravitational-wave signal. A safe auxiliary channel should not respond  
333 to these injected waveforms in  $h(t)$ . Then, we perform a statistical analysis of the  
334  $\mathcal{O}(5000)$  auxiliary channels sampled above 16 Hz using the `pointy-poisson` tool [40]  
335 to classify auxiliary channels as either “safe” (i.e., acceptable to use to veto potential  
336 gravitational-wave events) or “unsafe.” The resulting list of safe channels is then passed  
337 on to downstream data-quality analyses.

338 The injection and safety analysis process was repeated every few months in each  
339 detector during Engineering Run 15 (ER15) (April 26, 2023 - May 24, 2023) and O4a  
340 (May 24, 2023 - January 16, 2024) to track possible changes in safety and to ensure that  
341 any new channels were correctly classified as either safe or unsafe. During the first set  
342 of analyses in ER15, a handful of LHO channels were found to be unsafe compared to  
343 the existing list from O3: the electrostatic drive (ESD) voltage monitors at X-arm end  
344 station, and a handful of suspension rack magnetometers.

345 We found no substantial changes in channel safety during the subsequent duration  
346 of ER15 and O4a.

347 *2.1.5. Narrow spectral artifacts* A typical daily-averaged, high-resolution spectrum  
348 ( $\Delta f = 1/1800$  Hz) at either LHO or LLO reveals hundreds or thousands of narrow  
349 spectral artifacts (lines) within 10-2000 Hz, the band of particular interest to persistent  
350 gravitational-wave searches. These lines display a variety of amplitudes, widths, and  
351 shapes. Some are stable over long periods of time (weeks, months), while others are  
352 variable. Identifying and mitigating the most problematic lines requires both routine  
353 monitoring and focused investigations.

354 Since noise lines impact continuous gravitational-wave (CW) and stochastic  
355 gravitational-wave searches in slightly different ways, specific tools are used to evaluate  
356 these artifacts to aid the analyses. CW-focused line studies typically use a tool

357 called **Fscan** [41], while stochastic-focused studies use tools called **STAMP-PEM** [42] and  
 358 **StochMon** [43]. These tools provide complementary information about lines, and their  
 359 results are often used together to inform line investigations, mitigation efforts, and  
 360 data-quality products.

361 *Line investigations with Fscan* **Fscan** produces high-resolution spectra averaged over  
 362 long periods of time. It was largely rewritten for O4: modernizing the code, improving  
 363 stability of data generation, making new data products and visualization tools available  
 364 for analysis, and enabling production of custom spectra. In O4a, **Fscan** was used to  
 365 generate daily, weekly, and monthly spectra for about 80 channels at each observatory  
 366 site, using fast Fourier transforms (FFTs) of 1800-s-long data segments. Additional  
 367 analyses were performed to track lines of interest (determining witness channels and  
 368 times at which the artifacts changed) using **Fscan** data.

369 In section 2.2.7, we highlight examples of successful investigation and mitigation  
 370 efforts in O4a at LHO. Because LLO has generally cleaner data for persistent  
 371 gravitational-wave searches, there have been fewer notable examples of mitigation. A  
 372 number of high-priority narrow spectral noise artifacts, however, have not yet been  
 373 mitigated, including artifacts present at both detector sites. Additional work is ongoing  
 374 in this area. The highest-priority artifacts are those that contaminate a broad spectral  
 375 region (i.e., combs, especially those with many visible peaks) and artifacts that are  
 376 present at both sites (e.g., 60 Hz power mains) because these have a disproportionate  
 377 impact on persistent gravitational-wave searches.

378 The highest line artifacts in figure 1 have known cause, typically due to choices  
 379 inherent to the detector design (mirror suspension resonances at various frequencies,  
 380 strongest at 300 Hz and 500 Hz and harmonics) or calibration and dither lines to monitor  
 381 or control interferometric cavities, respectively.

382 *Monitoring strain-strain narrow-band coherence.* Stochastic searches rely on cross-  
 383 correlating  $h(t)$  data from detector pairs, so understanding and monitoring potential  
 384 noise sources that could detrimentally impact the cross-correlated data is crucial. A  
 385 stochastic monitoring tool called **StochMon** is specifically designed to calculate strain-  
 386 strain coherence in medium-latency (daily pages produced within 24 hours) and flag  
 387 problematic frequency bins that have excess coherence. The expected random coherence  
 388 between Gaussian datastreams is defined as the inverse of the effective number of  
 389 segments averaged to produce the coherence spectrum,  $1/N_{\text{eff}}$ ; in the case of **StochMon**,  
 390 Welch averaging with a 50% overlap is used between consecutive segments (for details  
 391 on the  $N_{\text{eff}}$  calculation see App. A of [44]). Frequency bins are flagged when they exceed  
 392 a Gaussian coherence threshold of

$$393 \gamma = 1 - \left( \frac{1}{N_f} \right)^{1/(N_{\text{eff}}-1)}, \quad (3)$$

394 where  $N_f$  is the number of frequency bins. An example of the calculated coherence  
 395 and its outliers is shown in figure 7. The outlier bins shown have all been traced back

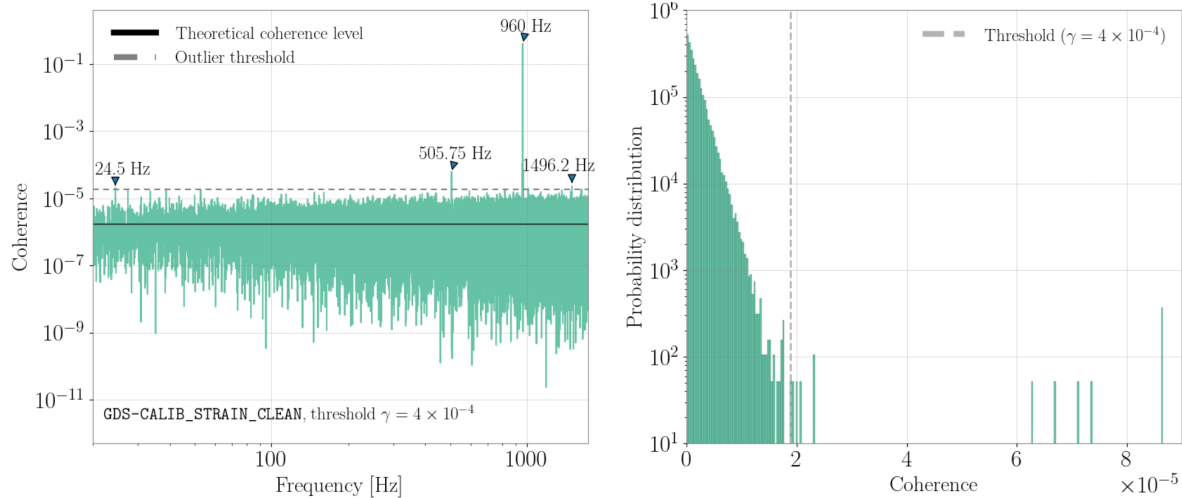


Figure 7: Left panel: coherence spectrum between LHO-LLO interferometer strain readouts. Right panel: histogram of the spectrum from StochMon.

396 to specific detector noise sources. The 505.75 Hz and 1496.2 Hz outliers lies within to  
 397 the first and third violin modes of the detectors, which are resonances of the detector's  
 398 mirror suspension fibers and are caused by changes in the fiber tension. The 24.5 Hz  
 399 outlier corresponds to a calibration line that was turned on between July 25, 2023 to  
 400 August 9, 2023 [45]. The 960 Hz outlier is caused by one of the DuoTone signals in both  
 401 LIGO detectors from the timing system, which is used to synchronize data collection  
 402 across the global detector network and within individual interferometers. [46].

403 In practice, the investigation to determine the instrumental causes of the coherence  
 404 outliers is crucial. They are carried out by spectral monitoring tools including `Fscan`,  
 405 and `STAMP-PEM`. `STAMP-PEM` is another stochastic monitoring tool that keeps track of  
 406 daily and weekly coherence between  $h(t)$  and physical environmental channels at 0.1 Hz  
 407 resolution. In terms of computing resources, a moderately low resolution of 0.1 Hz allows  
 408 it to monitor a wide range of channels (about 1000 channels per observatory site). The  
 409 high-resolution spectral information from `Fscan` and auxiliary channel information from  
 410 `STAMP-PEM` provide complementary information to support the strain-strain coherence  
 411 outliers investigation.

#### 412 2.1.6. Broadband persistent artifacts

413 *Investigations of coherence noise* Correlated magnetic noise was investigated as a  
 414 potential noise source for stochastic searches. During O4a, two sets of coordinated  
 415 magnetic injections between the two LIGO interferometers were performed to study  
 416 the coupling between the coherence of  $h(t)$  in the presence of an increased correlated  
 417 magnetic field, thereby determining the magnetic noise budget. The first set of injections  
 418 lasted 5 minutes and was composed of broadband white noise to test the synchronous  
 419 injections capability between the sites. The second set lasted approximately 45 minutes

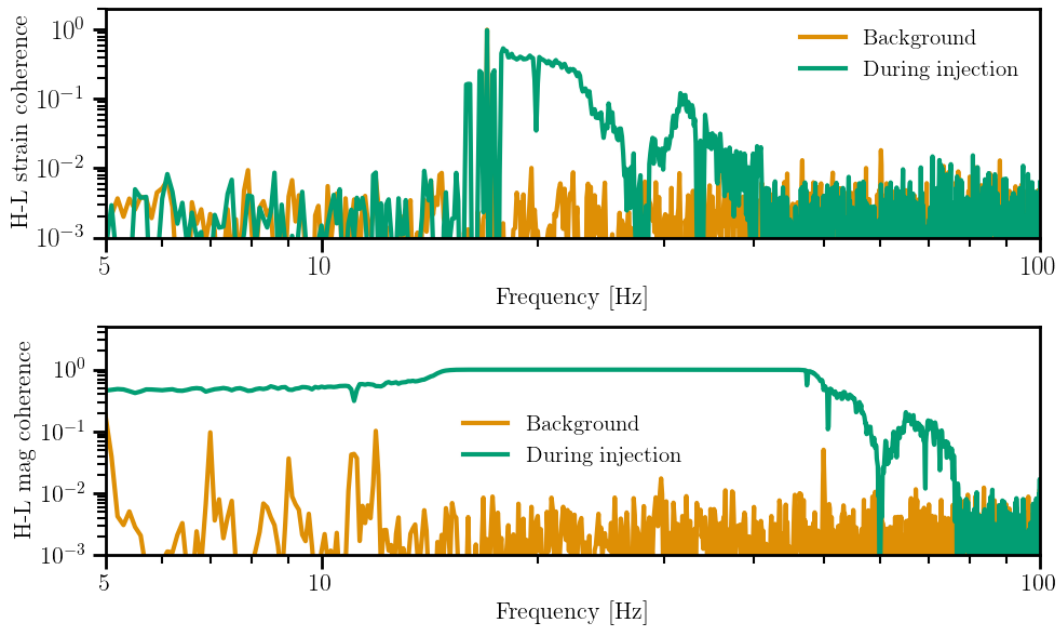


Figure 8: Coherence spectrums between LHO-LLO  $h(t)$  (top panel) and LHO-LLO magnetometers (bottom panel) during the correlated magnetic injections with Schumann-like spectrum, and the reference background time taken on December 21, 2023.

and consisted of a spectrum with Schumann-like frequency characteristics but at a significantly higher intensity ( $\sim 100$  pT in comparison with a realistic amplitude of Schumann resonance magnetic field of  $\sim 1$  pT) (see e.g., [47] for a description of Schumann noise relevant for ground-based gravitational-wave detectors). Figure 8 shows the coherence spectra between the x direction magnetometers in Laser and Vacuum Experimental Area in the corner station as well as the coherence between  $h(t)$  at LHO and LLO during the second set of injections compared to a reference background time. Details on the level of correlated magnetic noise estimate will be provided in the O4 stochastic analyses release.

## 2.2. LIGO Hanford noise investigations

**2.2.1. Electronics ground noise** During the commissioning period before O4, spectra of the variation in current flowing from building electronics ground to neutral earth were observed to be correlated with noise in  $h(t)$ . A newly developed electronics ground injection system showed that noise in  $h(t)$  could be produced by injecting  $\sim 100$  mA currents onto the building electronics ground. The coupling is thought to be produced by fluctuations in the potential of the electronics ground system due to the variations in current flows across the finite resistance between electronics ground and true neutral earth, measured to be about  $2 \Omega$  at LHO [48]. Forces on the charged test mass may fluctuate with the potentials of nearby electronic systems that are referenced to the

439 fluctuating electronics ground, such as the electrostatic drives (ESDs) and ring heaters.  
440

441 The noise from electronics ground potential fluctuations was reduced in two ways.  
442 First, the resistance between certain electronics chassis and the building electronics  
443 ground were reduced in order to reduce the total resistance to neutral earth for those  
444 electronics. At LHO it was found that lowering the resistance on the grounding wires for  
445 electronics chassis used to control test mass motion made the electronics less sensitive  
446 to ground potential fluctuations [49, 50]. Changing the grounding of controls chassis  
447 located at the end stations lowered the noise in  $h(t)$  overall and also reduced coherence  
448 between test mass motion and current to ground below 100 Hz [48].

449 Second, the biases of the ESDs were swept and set to values that minimized  
450 the coupling to  $h(t)$  of injections onto the electronics ground. It is thought that, at  
451 the coupling minimum, the forces on the charged test mass due to ground potential  
452 fluctuations are partially canceled out by an opposite dipole force associated with the  
453 bias-polarization of the test mass [48]. Sensitivity to ground potential fluctuations was  
454 therefore further reduced by selecting a bias voltage for the DC component of the ESDs  
455 which minimized coupling between  $h(t)$  and currents injected onto an electronics chassis  
456 at each end station [48].

457 These mitigations resulted in BNS range improvements of a few megaparsecs. The  
458 effects of these two changes on  $h(t)$  at LHO is illustrated in figure 9. Further mitigation  
459 could be obtained by shielding electronics inside the chamber from the test mass with  
460 shields that are connected to the chamber so that charges can rearrange to cancel  
461 the low-frequency fields produced by the electronics. The bias voltage that minimizes  
462 currents coupling to  $h(t)$  changes over time and continues to be tracked [51].

463 A minimum noise setting for Y-end ESD bias was identified at LLO before O4 [52]  
464 and midrun changes in the X-arm end station-end ESD bias were found to reduce noise  
465 at  $\sim$ 11 Hz and  $\sim$ 60 Hz and harmonics of these frequencies [53].

466 *2.2.2. Broadband transient noise* We noticed an increased noise at low frequencies  
467 which showed non-stationary behavior in the frequency band 10 – 50 Hz. A bicoherence  
468 analysis of  $h(t)$  noise with itself found that this noise was modulated by a low frequency  
469  $h(t)$  signal mostly around 2.6 Hz [54, 55]. Most of the longitudinal drive control to  
470 the ESD was being sent in the band 1 – 3 Hz which could have contributed to this  
471 increased noise. A new longitudinal control scheme that reduced the amount of control  
472 sent at these low frequencies was developed and implemented . This led to significant  
473 improvement in  $h(t)$  noise, thereby reducing the non-stationary or glitch behavior as  
474 well [56].

475 *2.2.3. Modifying input power* The amount of laser power input into the LIGO  
476 interferometers has increased in each Observing run. Increased power circulating in  
477 the arms improves the high-frequency sensitivity of the LIGO detectors by reducing the  
478 effect of quantum shot noise. In O4a, both LIGO detectors were slated to operate with  
479 75 W of laser power sent into the input mode cleaner (IMC).

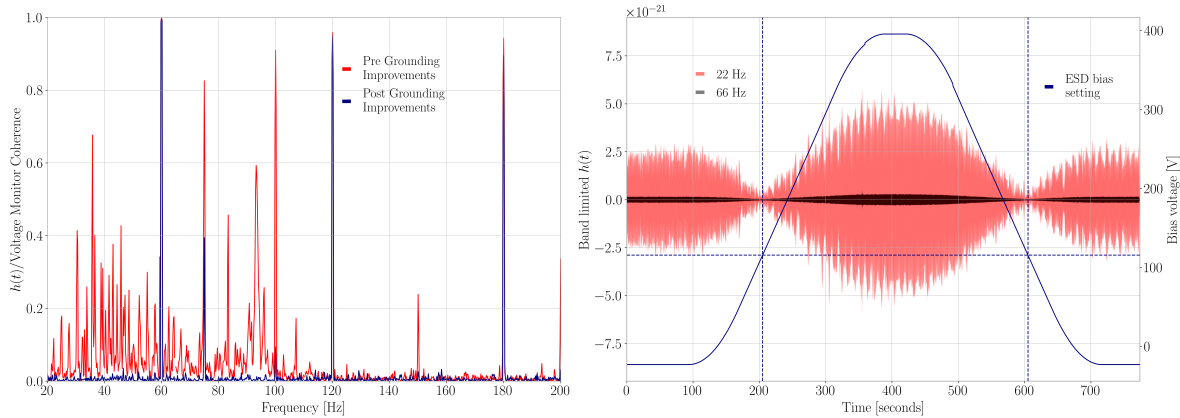


Figure 9: Two methods for reducing electronics noise in the GW data. Left panel: The coherence between the  $h(t)$  data and a temporary voltage monitor installed on a controls chassis at the X-arm end station [50]. Coherence between  $h(t)$  and chassis voltage decreased after changing the grounding wires used on controls chassis. Right panel: the bias voltage supplied to the ESDs is modulated, affecting the coupling of the harmonics of an 11 Hz comb injection. The new bias voltage was subsequently set to the value which minimized the amplitude of  $h(t)$  around the 11 Hz harmonics during the test [48]. Dashed lines show that that an ESD bias voltage of  $\sim 115$  V minimizes noise in  $h(t)$ .

479 As input laser power was increased at both detectors prior to the fourth Observing  
 480 run, vibration coupling also increased. This includes vibration coupling through both  
 481 scattered light noise and input beam jitter noise. A possible explanation is that  
 482 increased thermal distortion of the test mass surfaces around coating defects may  
 483 increase scattered light and also reduces the symmetry of the arms, decreasing common  
 484 mode rejection of input noise. The dramatic increases in coupling suggests that vibration  
 485 coupling may become increasingly problematic as input power is increased [37] in future  
 486 Observing runs and next-generation observatories.

487 Due to duty cycle and control scheme concerns associated with high-power  
 488 operation the laser power sent to the IMC was reduced from 75 W to 60 W at LHO  
 489 during O4a [57]. Figure 10 shows the reduction in vibrational coupling between PEM  
 490 sensors placed around the in-air optics table where the input laser light is produced and  
 491 the apparent differential arm length.

492 *2.2.4. Weekly magnetic monitoring* Regular measurements were taken before and  
 493 during O4a to understand the potential for coupling between local magnetic fields and  
 494 the interferometer [52, 58]. Local magnetic fields were generated by running a current  
 495 through large coils of wire mounted in the experiment hall and near electronics racks  
 496 used for interferometer controls [20]. The response of each interferometer to the resulting  
 497 magnetic fields was quantified using the network of PEM magnetometers set up around  
 498 each observatory [20, 59]. In order to vet GW candidates at kilohertz frequencies, such

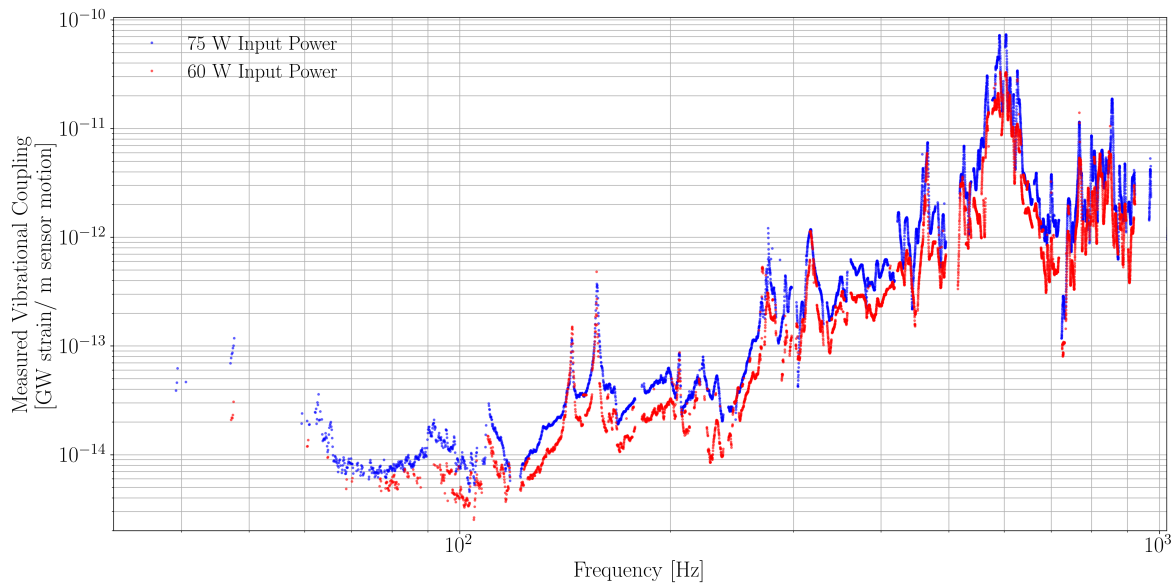


Figure 10: Comparison of the composite vibrational coupling function between PEM sensors placed around the pre-stabilized laser optics table measured during 75 W (blue) and 60 W (red) operation. The measured vibrational coupling at the input laser, observed where both the GW data channel and PEM channels witness a PEM injection [20], is worse at nearly all frequencies when operating at 75 W of input laser power.

499 as transients from neutron star f-modes [60–62], more computing space was allocated  
 500 prior to O4a to store accelerometer and magnetometer data up to 8192 Hz. Nearly every  
 501 week of O4a, a broadband magnetic field was injected at 1000 – 4096 Hz at 7 locations  
 502 around LHO for 36 s at each coil to quantify magnetic coupling in the newly-monitored  
 503 part of the kilohertz regime. These injections provoked a response in  $h(t)$  at the LIGO  
 504 LHO corner station. Figure 11 shows  $h(t)$  response to several of these weekly injections  
 505 compared to a reference background time. Weekly probes of the high frequency magnetic  
 506 coupling could be used to more accurately estimate the total environmental contribution  
 507 to a high-frequency GW candidate [63]. Broadband magnetic injections were also made  
 508 over 10 – 100 Hz and 100 – 1000 Hz from these 7 coils as part of the weekly injection  
 509 campaign.

510 During the course of O4a, the magnetic coupling of the detector at kilohertz  
 511 frequencies fluctuated from week to week. At the beginning of O4a, the LHO detector  
 512 was somewhat sensitive to large external magnetic fields applied at the Corner Station.  
 513 Towards the middle of O4a, the detector’s response to these applied magnetic fields  
 514 increased, before dropping to being only weakly coupled towards the end of O4a. The  
 515 most likely mechanism for the observed magnetic coupling in the kilohertz regime  
 516 is magnetic interference with cables that control the LIGO suspensions and optics.  
 517 Specific mid-run electronics configuration changes which affected the degree of magnetic  
 518 coupling, such as cables being rerouted, have not yet been identified.

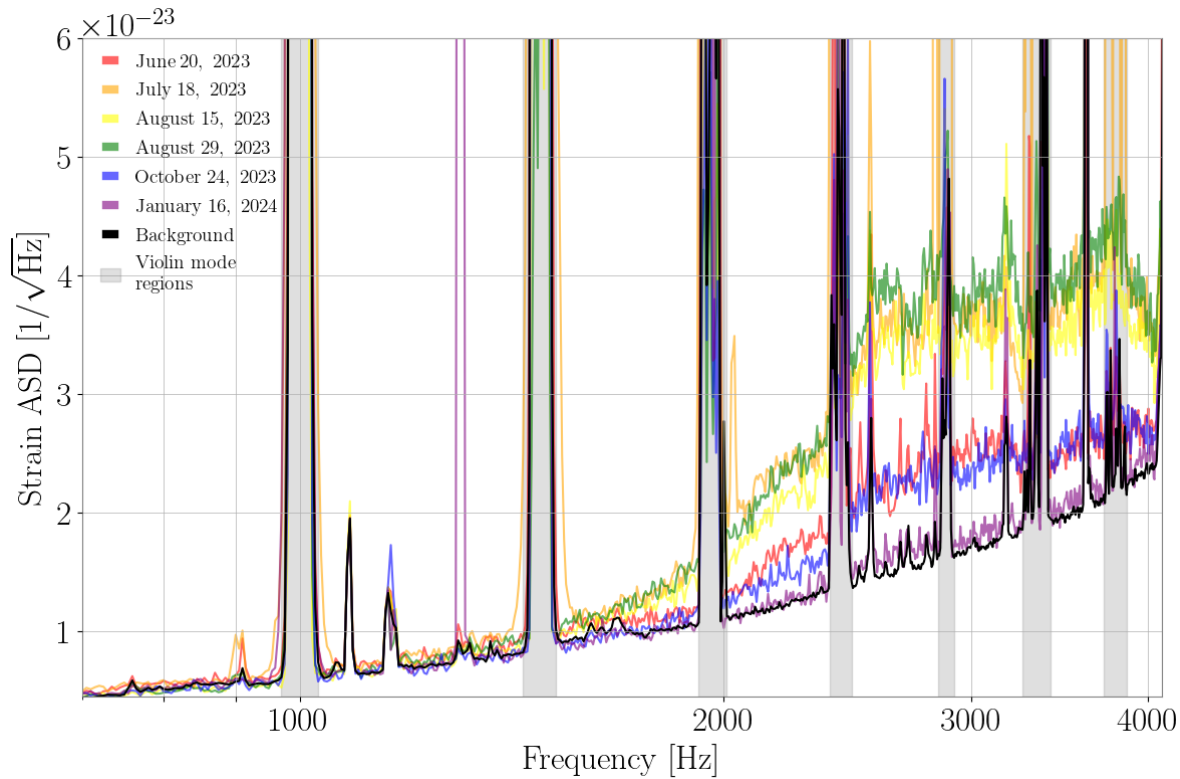


Figure 11:  $h(t)$  data from 6 of the 22 weekly high-frequency magnetic injections performed at the LHO corner station. Above  $\sim 2000$  Hz, there was a significant response in  $h(t)$  when a large external magnetic field was applied near the beamsplitter area during the middle portion of O4a. The reference background time was taken on June 20, 2023. The strain ASD also varied from week to week in certain frequency bands due to the relative absence or presence of excited thermal (violin) modes in the data. The violin mode frequency bands are denoted by the grey regions in the figure.

519 2.2.5. *Cosmic ray glitch correlations* A high energy cosmic ray shower is a potential  
 520 mechanism for creating glitches via momentum transfer to, heating of, or changing  
 521 the electric potential near the test masses [64, 65]. Cosmic rays are monitored by  
 522 four photomultiplier tubes placed beneath the vacuum chamber which houses the X-  
 523 arm input test mass at LHO. During O2 and O3, we compared the time difference  
 524 between cosmic ray arrival times and blip glitches at LHO and found no evidence of a  
 525 correlation [10]. We expanded this search in O4a to include blips, low-frequency blips,  
 526 repeating blips, and tomtes as identified by Gravity Spy [14]. A description of the  
 527 cosmic ray sensor systematics in O4a can be found at [66]. No temporal correlation was  
 528 found between cosmic rays and any of these glitch classes. Additionally, we found the  
 529 amplitude of cosmic rays which struck LHO within a second of a glitch were consistent  
 530 with the overall amplitude distribution of cosmic rays witnessed by the cosmic ray  
 531 detectors installed at LHO.

532 *2.2.6. Scattering noise from the input arm* In O4a, short shutdowns of the LHO  
533 building heating, ventilation, and air conditioning (HVAC) system produced several  
534 percent increases in astrophysical range [67]. Localized vibration injections indicated  
535 that the coupling of the HVAC vibrations at the corner station was in the input arm of  
536 the interferometer [68]. The coupling was further localized by using broad-band shaker  
537 injections to increase the amplitude of vibrations above ambient levels so that laser  
538 vibrometry could be used to identify the internal structures that had resonances that  
539 were characteristic of the scattering noise [69]. During the O4a-O4b break, the baffles  
540 were moved and damped, and new baffles added, greatly reducing the vibration coupling  
541 in the input arm [70, 71].

542 *2.2.7. Comb investigations* During O4a, two sources of comb artifacts were identified  
543 and mitigated at LHO. The first source was in the electronics driving a mirror heating  
544 element. This created a comb of approximately 1.6611 Hz (though different mitigation  
545 efforts caused changes in the spacing) centered around 280 Hz. A time-correlation was  
546 found between changing electronic settings for the mirror heating element and variations  
547 in the 1.6611 Hz comb amplitude, which suggested a possible source for the comb [72].  
548 This insight motivated subsequent mitigation efforts that more clearly identified the  
549 problem. Electrical connections were changed to stop the 1.6611 Hz comb from being  
550 created [73].

551 The second source created a near-1 Hz comb, as well as a near-5 Hz and near-7 Hz  
552 comb at various times. All three combs were traced to Hartmann wavefront sensors  
553 (HWS), which are part of the interferometer alignment sensing and control (ASC)  
554 subsystem [74]. It was determined that the comb frequency spacing changed when  
555 the HWS camera shutter frequency setting was changed [75, 76]. The low amplitude  
556 of the comb makes observing this artifact in short stretches of data (less than  $\sim$ 1 day)  
557 challenging, and thus mitigation efforts more time-consuming. Once the connection  
558 between changes in the comb spacing to changes in HWS hardware settings was  
559 established, efforts to change the hardware configuration while in observing mode helped  
560 to mitigate this comb [77].

### 561 *2.3. LIGO Livingston noise investigations*

562 *2.3.1. Slow scattering* Noise due to high ground motion in the band 0.1–0.5 Hz was  
563 the most dominant source of glitches in the LLO data during O4a. These glitches, also  
564 known as Slow Scattering, adversely impacted the strain sensitivity mostly in 10–50 Hz  
565 band. Figure 12 shows glitch rate and ground motion for three days. For two of these  
566 days, ground motion in the band 0.1–0.5 Hz was high, which led to a high rate of Slow  
567 Scattering glitches in the data.

568 The additional phase noise as given by (2) shows up as arches in the time-frequency  
569 spectrogram as shown in the middle plots in figure 2. The time separation between  
570 subsequent scattering arches gives a direct measure of the frequency with which the

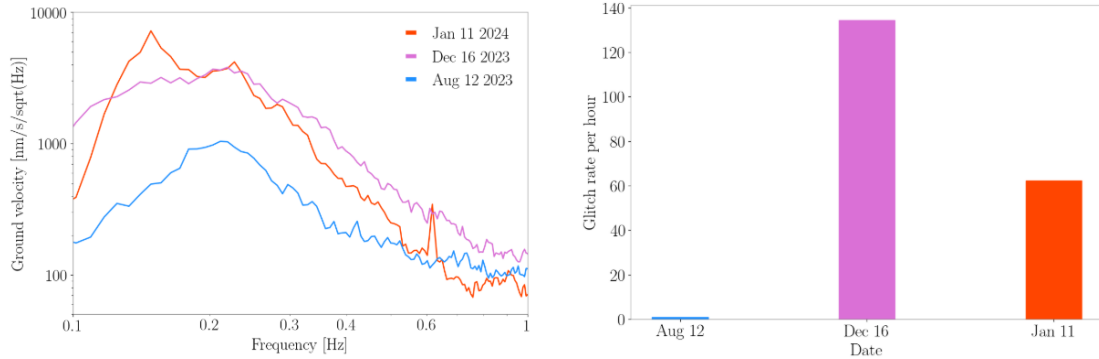


Figure 12: Left panel: Ground motion in the 0.1–1 Hz frequency band during different days of O4a. Right panel: Hourly rate of glitches in the frequency band 10–60 Hz and SNR in between 20 and 200 during the same days.

571 scattering surface is moving. During O4a, we have seen that the frequency of the  
 572 scattering surface is not constant because it moves at whatever frequency is dominant  
 573 in the ground motion [34]. We have not yet found any optics which have enough velocity  
 574 to create noise above 10 Hz in  $h(t)$ .

575 *2.3.2. Fast scattering* During O3, Fast Scattering glitches were the most common  
 576 glitch source at LLO, making up about 27% of all glitches with a confidence of 90%,  
 577 according to Gravity Spy [14, 15, 24]. Fast scattering is typically found to be correlated  
 578 with ground motion in the microseismic band 0.1–0.3 Hz, and the anthropogenic band  
 579 1–6 Hz. Fast scattering arches are short in duration, shown in figure 2, and impact the  
 580 detector sensitivity in the 10–100 Hz frequency range. Trains, logging, construction, and  
 581 other human activity were the main sources of Fast Scattering, as the anthropogenic  
 582 motion upconverts to higher frequency [15, 18].

583 In O3, trains near the LLO Y-arm end station produced low-frequency seismic noise  
 584 that would upconvert into the gravitational-wave sensitive frequency band [78]. For this  
 585 reason, they provided an avenue to study how periods of large ground motion impacted  
 586 the detector. Spectrograms of the ground motion revealed many harmonic lines with  
 587 changing frequency, and short bursts of increased amplitude in the strain data. The  
 588 suspicion was that each burst was produced by the low-frequency ground motion exciting  
 589 mechanical resonances of some scattering surface. Two methods, Lasso regression [79]  
 590 and Spearman correlation [80], were employed to identify which narrow band seismic  
 591 frequencies contributed the most to increased detector noise. Both methods consistently  
 592 pointed to ground motion in the 1.8–2.2 Hz range as the primary factor correlating with  
 593 heightened strain noise at the corner station [78]. The subsequent mitigation of noise  
 594 from these frequencies for O4 is discussed in section 2.3.3.

595 From roughly June 2023 through August 2023, there was a significant amount

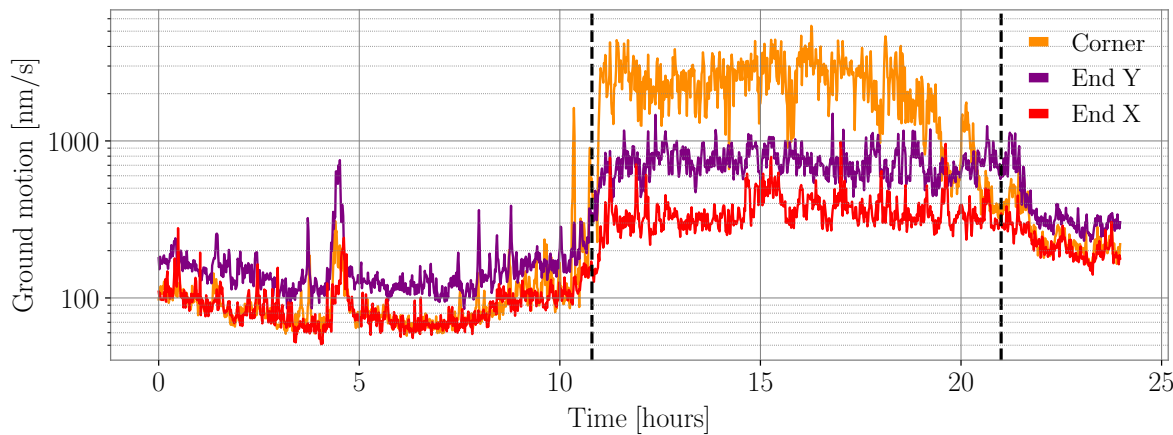


Figure 13: Example of a day in which LLO lost lock due to nearby logging activities. Each trace represents band-limited RMS data from 1–3 Hz taken from seismometers at the X-arm end station, Y-arm end station and corner station. The detector could not be locked for roughly 10 hours, indicated by the dashed lines, as ground motion levels in the vertical direction surpassed 1000 nm/s at the corner station. In local central time, the elevated ground motion was from roughly 6am to 4pm.

596 of logging occurring near LLO [81, 82]. The anthropogenic ground motion in the  
 597 vertical direction near the corner station consistently reached amplitudes greater than  
 598 1000 nm/s, as shown in figure 13. These high ground motion levels caused the detector  
 599 to lose lock multiple times for many hours during the daytime. After August 2023, the  
 600 logging activity ceased, significantly reducing the disruptive ground motion near the  
 601 corner station.

602 *2.3.3. Arm cavity baffle resonances* Arm cavity baffles (ACBs) [83] are located at each  
 603 of the test masses, attached to the first stage of the active seismic isolation system  
 604 (hydraulic external pre-isolator (HEPI) [84]), and are used to catch the light from wide  
 605 angle scattering. Arm cavity baffle (ACB) resonances are sensitive to the physical state  
 606 of the system and changes to it can lead to the shift in resonant frequencies [18]. After O3,  
 607 but before O4, at the corner and Y-arm end station, the ACBs had a high-quality-factor  
 608 resonance at around 1.6 Hz [85]. When rung up, noise appears in the gravitational-wave  
 609 data from around 20–100 Hz. In the absence of high microseismic ground motion, 1.6 Hz  
 610 motion would create scattering noise at 3.2 Hz. After O3 ended, 3.3 Hz scattering noise  
 611 was observed that had not been seen before; this can be explained by ACB resonances at  
 612 1.6 Hz. We suspect that during O3, the ACB resonance was around 2 Hz, which would  
 613 produce the common 4 Hz Fast Scattering observed. In late 2022, the ACB resonances  
 614 at the corner and Y-arm end station were mechanically damped. As a result, the rate  
 615 of Fast Scattering decreased dramatically and subsequently it was found that this noise  
 616 coupling was no longer present [18]. The effect of this remediation can be seen in the  
 617 sweep injections performed in July 2022 (see figure 14) using a shaker and again in

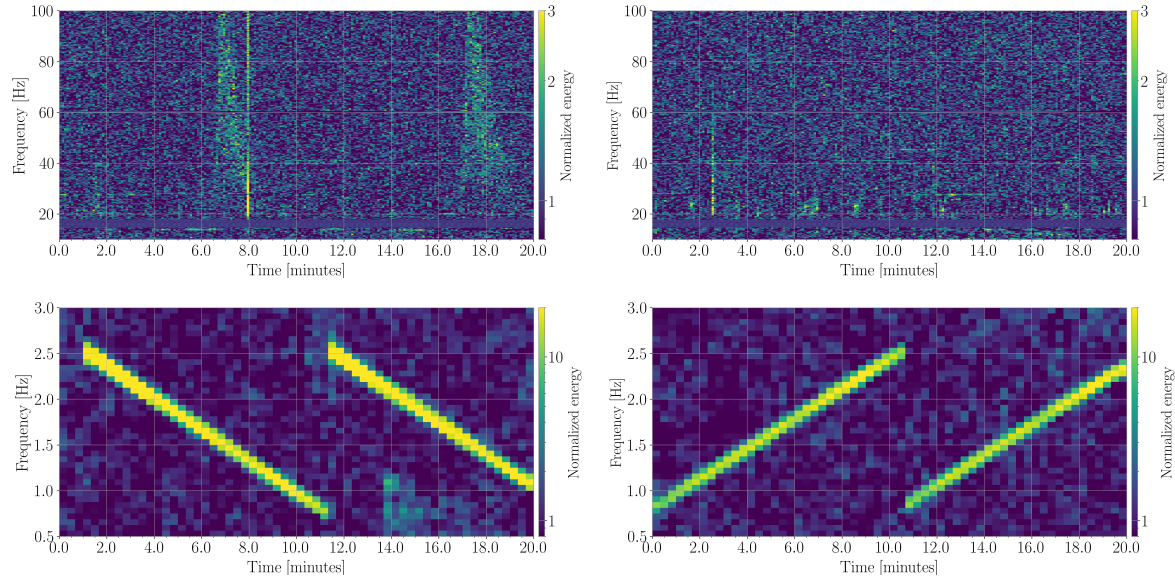


Figure 14: Sweep test comparison before and after the damping of the ACB [87]. The top spectrograms show the strain noise, and the bottom spectrograms show the sweep injections performed on the corner station HEPI. After the ACB was damped, we no longer observed increased strain noise due to mechanical resonances.

618 February 2023 [86].

619 Comparisons of the impact of logging during O3 and O4 showed that for similar  
 620 ground motion amplitudes, the rate of transients was significantly reduced by a factor  
 621 of about 50 [18]. In O3, anthropogenic ground motion at such high levels would have  
 622 produced many glitches detected by Omicron (assuming lock is not lost). Due to the  
 623 damping of the arm cavity baffles, we did not observe significant strain noise due to the  
 624 logging activities in O4 [88].

625 *2.3.4. Binary neutron star range oscillations* During O4a, from time to time, the  
 626 observed BNS range exhibited oscillations with a period of about 30 minutes and a  
 627 range variation of about 5-15 Mpc, lasting for all or part of a day. These variations can  
 628 be seen in figure 15. The range variations are the result of broadband excess noise in  
 629  $h(t)$ .

630 Searches for the cause of these oscillations identified accelerometers that seemed  
 631 to witness motion that aligned with the oscillations [89–91]. There is a line at around  
 632 30 Hz produced by the HVAC system, and initial investigations hypothesized that this  
 633 line changing amplitude could be responsible for the observed BNS range oscillations.  
 634 To check, a shaker injection at 30.5 Hz was performed on the vacuum enclosure of the  
 635 chamber containing the X-arm end test mass. The 30.5 Hz shaker injection could not  
 636 re-create the broadband effect we observe in  $h(t)$  [92].

637 The hunt for what may be causing these oscillations was continued by analyzing  
 638 the output of the summary page tool Lasso. As described in [93], Lasso can produce

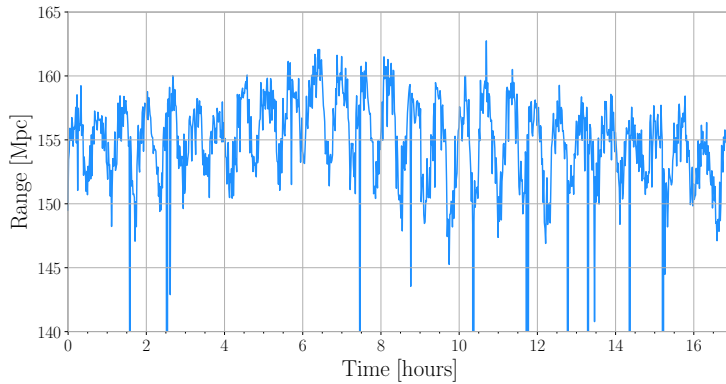


Figure 15: Range variations as observed on Dec 23 2023 at LLO. The variations are present for most of the day, and the magnitude of the drops ranges from roughly 5-10 Mpc.

639 overlays of the BNS range with auxiliary channels, allowing identification of channels  
 640 with similar periodicity to the range variations. However, range variations often include  
 641 secular trends combined with the oscillations, such that the channels found by Lasso  
 642 often fail to align with the period of the oscillations and are thus unlikely to yield  
 643 information about their cause.

644 The channels that seemed to correlate the most, according to the Lasso algorithm,  
 645 were primarily located at the X-arm end station and were related to temperature sensors.  
 646 Additional days with similar leading channels were found – along with channels not  
 647 explicitly measuring temperature but sensitive to it [94]. Additional investigations have  
 648 mentioned issues with temperature control [95]. While the evidence seems to implicate  
 649 temperature effects at the X-arm end station, a deeper study during all of O4a could  
 650 not yield the actual cause, as the oscillations are still present in O4b. The coupling  
 651 mechanism between the thermal variations and  $h(t)$  is not currently known.

652 *2.3.5. 84 Hz  $h(t)$  noise* During ER15, excess noise around 84 Hz in  $h(t)$  data was  
 653 present. The noise would appear and disappear, suggesting that its cause might be  
 654 related to dehumidifiers and fans which turn off and on.

655 This noise was present in accelerometers at both end stations, but was louder at the  
 656 Y-arm end station. Analysis of spectrograms and outputs of the channels that monitor  
 657 dehumidifiers and fans pointed towards the 84 Hz source being related to two exhaust  
 658 fans located at the Y-arm end station [96]. To further confirm that this excess noise is  
 659 coming from the Y-arm end station, broadband acoustic injections were done at both  
 660 the X-arm end station and the Y-arm end station. These injections revealed a sharp  
 661 mechanical resonance at around 84 Hz at the Y-arm end station [97]. The exact coupling  
 662 mechanism of the fans into  $h(t)$  is still unknown, but the source was removed by moving  
 663 the fans off the beam tube enclosure doors [98].

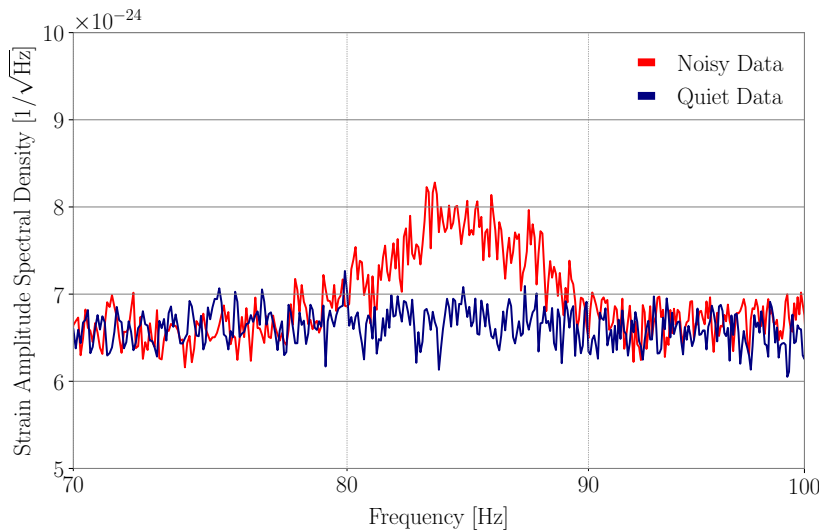


Figure 16: Comparison of data in which excess noise was present at around 84 Hz on March 2, 2023, seen here as a visible ‘‘bump’’. The quiet data is taken from the same day when this noise was absent in  $h(t)$ .

### 664 3. Event Validation in O4

665 Validation of GW candidates is a crucial step that enhances our confidence in the  
 666 astrophysical origin of the candidate events and the reliability of source parameter-  
 667 estimation results. Event Validation refers to the process of checking for the presence of  
 668 any data-quality issues surrounding the time of an event and conveying this information  
 669 to the relevant data analysis groups in the collaboration. These assessments build  
 670 upon the initial vetting conducted by the Rapid Response Team (RRT), a joint LSC-  
 671 Virgo-KAGRA Collaboration (LVK) working group tasked with promptly responding  
 672 to event candidate alerts [6]. The RRT conducts a series of prescribed data-quality  
 673 checks, informed by the Data Quality Report (DQR); see section 3.1, and verifies the  
 674 overall functioning of the low-latency pipeline infrastructure. This team provides round  
 675 the clock coverage, comprising rotating on-shift scientists and experts from the various  
 676 areas of detector operations, including DetChar. The prompt assessment, made after  
 677 the alert for a significant event is produced by online searches, is then reconsidered  
 678 more thoroughly and in more detail by the Event Validation task force to determine  
 679 a final evaluation of the data-quality for every event candidate. Multiple checks are  
 680 performed on the data, e.g., making sure the detector is operating in a nominal data-  
 681 taking configuration, identifying any noise artifacts that could bias source property  
 682 estimation, and checking for any inconsistencies in the output of the PEM sensors as  
 683 that may suggest noise coupling between the environment and strain data. If the data-  
 684 quality around the candidate event is found to be unsatisfactory, further data processing  
 685 techniques such as bayesian noise inference and transient noise removal may be applied  
 686 [99]. For example, BayesWave data cleaning and linear noise subtraction were applied to

687 a total of 17 events during O3. The catalog papers discuss these events and techniques  
688 in more detail [100–102].

689 There have been a number of changes and improvements in the event validation  
690 procedure since the last observation run. These changes include:

- 691 • An LVK event validation roster for all active detectors: O4a event validation  
692 infrastructure is designed to take information from LIGO, Virgo and KAGRA  
693 interferometers. This centralization has reduced the person power and time  
694 required to perform event validation compared to past Observing runs, during  
695 which the LIGO and Virgo Collaborations conducted validation of their detector  
696 data separately [12, 103]. Additionally, the unified framework has ensured more  
697 standardization and uniformity in the procedures for evaluating data-quality and  
698 the tools utilized for the assessment.
- 699 • More automated event validation software infrastructure: The event validation  
700 infrastructure in O4 is centralized and is maintained using git version control  
701 on the event validation website, accessible to all LVK members. This centralized  
702 infrastructure allows easier information flow from DQR, to noise mitigation teams  
703 and other data analysis groups. The event validation website acts as a repository  
704 of all the details related to event validation including a list of events, the contact  
705 information of the volunteers and RRT experts, links to event’s DQR report and  
706 the event validation. For each event, an issue page is created where any additional  
707 details regarding the event’s data-quality can be discussed. This page is also linked  
708 from the Event validation website.
- 709 • More automated DQR infrastructure: The DQR is a DetChar tool used to assess the  
710 data-quality surrounding an event time, as detailed in section 3.1. The O4 version  
711 of the DQR has undergone significant upgrades compared to O3, incorporating  
712 automated checks that offer insights into the interferometer’s state and data-quality  
713 around the event time. The results of these checks are displayed in the form of labels  
714 (Pass, Data Quality (DQ) issue, or Task fail), indicating whether a particular data-  
715 quality check has been successful or not. The event validation volunteers in O4  
716 have made extensive use of these results for validation purposes.

### 717 3.1. Data Quality Report

718 As mentioned, the primary tool used in event validation is the DQR [104]. In O3, similar  
719 DQR toolkits were separately used by the LIGO Scientific Collaboration (LSC) [12]  
720 and Virgo Collaboration [105] to evaluate candidates from the GWTC catalog. For  
721 O4, we used the experience gained from O3 to improve the DQR, with a focus on  
722 improving the speed and robustness of analyses, increasing the fraction of analyses that  
723 were automated, and generalizing the software to support analysis of data from all  
724 ground-based gravitational-wave detectors. One key upgrade was the use of a p-value,  
725 which is the probability of failing to reject the null hypothesis, to automatically identify  
726 data-quality issues that could impact the detection or analysis of gravitational-wave

727 candidates. Additional details about the DQR architecture used in O4a can be found  
728 in [104].

729 A wide variety of different analyses were used as part of the DQR framework  
730 during O4a. Tests that were used to analyze LHO and LLO data include: estimates  
731 of noise contributions from the observatory environment [63], statistical correlations  
732 between strain data and auxiliary-channel information [28], predictions of the presence  
733 of glitches using only auxiliary information [106], analytic identification of excess power  
734 in spectrograms of the strain data [107, 108], machine-learning image classification of  
735 spectrograms of the candidate [109], quantitative estimates of the data stationarity [110],  
736 estimates of the Rayleigh statistic of the data, measurements of the local glitch rate [111],  
737 and monitors of the detector range at the time of the candidate. These tasks were  
738 completed on two different timescales. Most tasks were completed within 5 minutes  
739 of a DQR being launched, allowing these tasks to be used as part of the initial rapid  
740 response to identified gravitational-wave signals. Additional tasks were available within  
741 a few hours to help with additional offline event validation of each candidate.

742 A key feature of this updated DQR was the ability to automatically flag DQ issues  
743 in the candidate events identified by tasks based on the reported p-value. Candidates  
744 with DQ issues reported by the DQR underwent additional scrutiny as part of the  
745 rapid response to gravitational-wave candidates in O4a. No additional human follow-up  
746 of the candidate data-quality was completed in low latency when no DQ issue was  
747 identified. All candidates were further analyzed offline, however, regardless of the  
748 conclusion reached in low latency.

749 We found that the choice of p-value threshold strongly impacted the rate of false  
750 alarms from the DQR. The p-value threshold chosen to identify a data-quality issue was  
751 changed partway through the run for this reason; at the start of O4a, a threshold of 0.1  
752 was used, but was eventually changed to 0.05. This lower threshold reduced the rate  
753 of false alarms with minimal reduction in the true alarm rate. We also changed the set  
754 of tasks used throughout the run to improve the true alarm rate and reduce the false  
755 alarm rate. Using a single p-value threshold was also suboptimal, as the exact definition  
756 of the reported p-value varied between tasks. This led to tasks either overreporting or  
757 underreporting the presence of DQ issues. This limitation has been addressed for O4b  
758 by introducing task-specific thresholds that are informed by our O4a experience.

### 759 3.2. Event Validation procedure

760 The Event Validation workflow is shown in figure 17. For each event, the volunteer  
761 (or volunteers) assigned to the week-long validation shift is (are) immediately notified.  
762 They receive all necessary information about the event, as well as instructions on how to  
763 validate it. This includes links to the Event Validation form, the DQR and the GraceDB  
764 (Gravitational-Wave Candidate Event Database) § page for the event. In the event  
765 validation form, the validator can fill the event details for each detector. These details

§ [www.gracedb.ligo.org](http://www.gracedb.ligo.org)

766 include the “validation conclusion for the detector”; the options are “Not Observing”,  
767 “No Data Quality Issues”, and “Data Quality Issues”. This information is then used  
768 as input for glitch subtraction before parameter-estimation analysis, as detailed in the  
769 next paragraphs. Once the validator is satisfied with their findings, they can submit  
770 the validation form. This validation conclusion is then passed to the noise mitigation  
771 review team.

772 The noise mitigation team is responsible for assessing whether any excess power  
773 within the target time-frequency analysis window of any candidate is sufficiently non-  
774 Gaussian to require further action [110, 112]. We do this by comparing the PSD noise  
775 variance in each identified time-frequency region and check it is consistent with Gaussian  
776 noise. For regions which are not consistent with Gaussian noise ( $p\text{-value} < 0.01$ ) there  
777 are two options available. If the noise is sufficiently isolated in time and frequency the  
778 noise transient can be subtracted from the data. All noise-subtracted data in O4a were  
779 produced by the BayesWave algorithm [99, 113]. The procedure of how this is done is  
780 described in the Appendix of Ref [6].

781 To assess the efficacy of the noise subtracted data we compare the Gaussianity  
782 of the noise-subtracted data within the targeted time–frequency window to Gaussian  
783 noise [107]. Noise-subtracted data consistent with Gaussian noise is deemed sufficiently  
784 stationary for parameter estimation. If the noise is extended in time and frequency  
785 such that noise subtraction is not appropriate, or the noise subtracted data were not  
786 sufficiently stationary, the noise mitigation team can recommend restricting the time-  
787 frequency analysis window, so the parameter estimation analysis does not take into  
788 account any of the noise. The final recommended time-frequency analysis window,  
789 along with the recommended data frame name, can then be sent through CBCFlow for  
790 parameter estimation to automatically retrieve the information and start their analyses.  
791 CBCFlow is a Python library that facilitates storage and transfer of event metadata  
792 [114].

### 793 3.3. Validation of O4a events found by online search pipelines

794 In O4a, online searches generated alerts for 92 significant event candidates. Out of  
795 these, 11 were retracted by the RRT due to evident contamination from noise artifacts  
796 or other issues that resulted in inaccurately estimated event significance, rendering their  
797 astrophysical origin improbable [115–125]. Some of the events from the remaining 81  
798 candidates required noise mitigation through glitch subtraction. The procedures for  
799 assessing the necessity of glitch subtraction and its execution, along with the evaluation  
800 of the result, are detailed in [112].

801 For the remaining events showing data-quality issues but deemed not to require  
802 glitch subtraction, restrictions were implemented on the analyzed times and frequency  
803 bands surrounding the events. A common problem was low-frequency non-stationary  
804 noise, particularly in the lowest part of the detector sensitivity range, between 10 and 40  
805 Hz, often caused by ground motion. Examples of this noise can be seen in the middle and

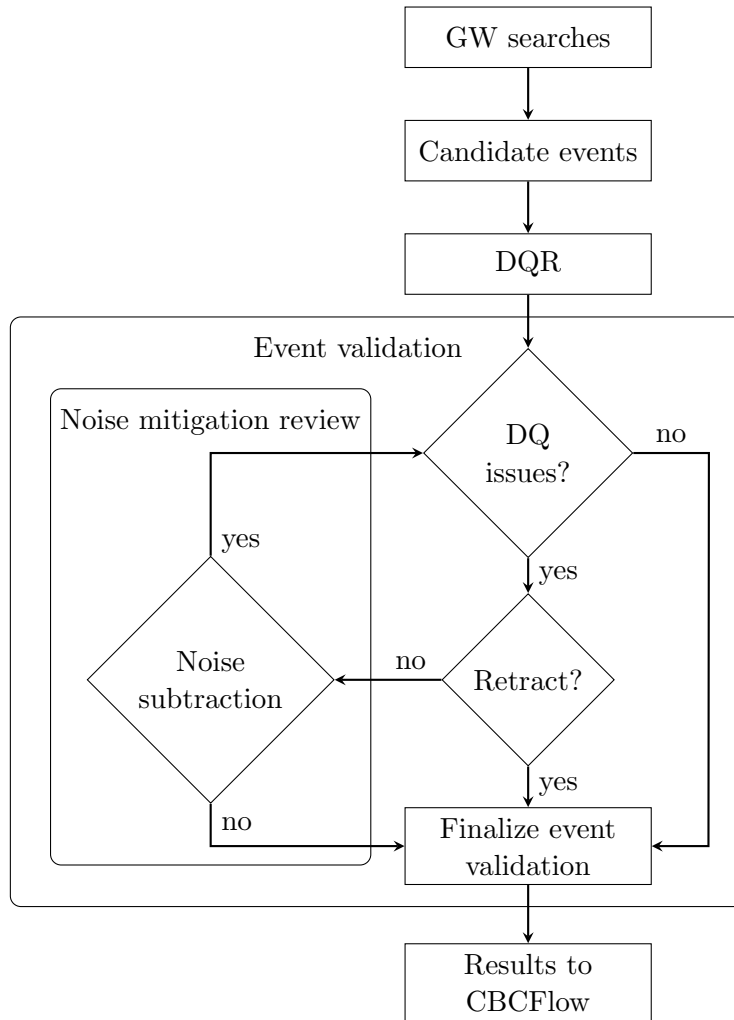


Figure 17: Event validation workflow. The DQR output is evaluated for data-quality issues. If none are found, the event is validated and the data proceeds to downstream analysis. If DQ issues are present, the event candidate may be retracted or noise subtraction recommended. The results of noise subtraction are then reassessed for residual DQ issues, repeating the evaluation process if needed.

lower panels of Fig. 2. While GW searches and parameter estimation typically start at 20 Hz [6] to avoid the noise wall below 15 Hz (as shown in Fig. 1), when non-stationary noise is present, the lowest frequency may be increased to exclude the affected frequency range and avoid biases in the analysis results.

#### 4. Data Quality for Astrophysical Searches

DetChar seeks to help mitigate or eliminate identified noise sources as a top priority. Since this is not always feasible and excess non-Gaussian noise remains in archival data even in cases where the issue was corrected, the DetChar group prepares various data-quality products applied to astrophysical searches to reduce the impact of non-

815 Gaussianity of the data on these searches.

816 *4.1. Data quality products for all searches*

817 As in previous observation runs [12], the LIGO DetChar group recommended that  
818 specific periods when the data is unusable due to severe data-quality issues be removed  
819 from analyzed data prior to performing astrophysical searches. This is handled through  
820 defining segments (time periods specified by start and stop times) to be vetoed by data-  
821 quality flags. Category 1 flags define times to be removed prior to running an analysis.  
822 It is generally recommended that a consistent set of these flags be applied across all  
823 searches, making them relevant for all analyses described in later subsections. Searches  
824 for gravitational waves have continued to become more sophisticated in their handling  
825 of suboptimal detector data, including utilization of noise subtraction techniques to  
826 extract gravitational-wave signals in data with noise transients present. For this reason,  
827 LIGO DetChar was less aggressive about recommending periods of data for removal  
828 through defining data-quality flags in O4a than in previous runs.

829 Periods of non-stationarity with significant salvageable data in some frequency  
830 bands were left in place. However, there were still stretches of data when the detector  
831 was nominally supposed to be operating as an astronomical observatory during which the  
832 data were in practice un-analyzable due to severe issues sufficient to bias the PSD or the  
833 detector status otherwise being inconsistent with the detection of gravitational-waves.  
834 The total deadtime percentage, defined as percentage of observation time removed by  
835 data-quality flags, was less than one tenth of one percent for each interferometer during  
836 O4a. Category 1 flags covered issues including:

- 837 • Incorrect line subtraction for the LHO or LLO, generally at the start of lock  
838 stretches.
- 839 • Parametric instability mode [126] rung up and severely impacting data shortly  
840 before causing lockloss. This issue occurred infrequently in both LIGO  
841 interferometers in O4a and also occurred in the third Observing run [12].
- 842 • A servo causing severe issues with squeezing [8] at LHO.
- 843 • Violin modes [127] rung up severely at LLO, in one case leading directly to distorted  
844 strain data followed by lockloss, and in another case causing issues with data  
845 calibration.
- 846 • Observing mode was defined incorrectly in either LIGO interferometer early in the  
847 ER15 Engineering run prior to O4a.
- 848 • Observing mode was defined but  $h(t)$  data was not stored permanently due to  
849 technical issues.

850 *4.2. Data quality for transient searches*

851 Searches for transient gravitational-waves cover gravitational-wave emission that will  
852 be in the detectable LIGO frequency band for relatively short duration (sub-second

853 to minutes). These searches include matched-filter analyses detecting compact binary  
854 coalescences (CBCs) as well as searches for less well-modelled phenomena referred to  
855 as GW bursts. In previous runs, both types of transient searches used Category 2  
856 flags, which are typically shorter in duration than Category 1 and targeted the needs  
857 of specific analyses. Due to improved confidence in gravitational-wave detection in  
858 the presence of noise, CBC searches have eliminated the use of traditional Category 2  
859 flags, although some of these searches use other supplementary data-quality products  
860 instead as described below. Unmodelled transient searches, which cannot rely on the  
861 characteristic chirp structure of the gravitational-wave signal for confirmation, continue  
862 to use these additional data-quality flags, but fewer kinds of flags, resulting in reduced  
863 deadtime compared to previous runs.

864 *4.2.1. Data quality for compact binary coalescence transient searches* The primary  
865 data-quality products used in CBC searches were the iDQ [106] timeseries. The  
866 iDQ pipeline produces statistical data-quality information based on auxiliary channel  
867 activity. In O4a, the Ordered Veto List (OVL) [128] algorithm was implemented within  
868 iDQ to create and rank an ensemble of vetoes for strain data triggered on auxiliary  
869 channels. The internal rank of OVL is then calibrated to probabilistic statements on  
870 the presence of a glitch by iDQ. To produce timeseries, the generated vetoes are applied  
871 to the strain data, and the probability that any time in the strain data contains a glitch  
872 is given by the highest ranked veto active at that time. These output timeseries are  
873 available for each detector in real-time and contain a number of statistics calculated  
874 by OVL for each time sample: the ranking statistic; the false-alarm probability (FAP),  
875 which is the probability that a random time with no glitch would be ranked at least as  
876 high as the current sample; the natural logarithm of the likelihood that transient noise  
877 is present ( $\log L$ ); and a state vector for iDQ indicating the quality of the iDQ data.

878 CBC searches in O4a were performed in two different operating modes, online and  
879 offline. In online operations, CBC detection pipelines search for gravitational waves in  
880 near real-time with initial low-latency alerts sent to the public for significant detections  
881 on a timescale of seconds to minutes. In offline operations, CBC detection pipelines  
882 analyze archival data in high latency on a timescale of weeks. These offline searches  
883 have data from the entire Observing period available to them as well as additional data-  
884 quality products such as the Category 1 vetoes described previously. This makes the  
885 offline configuration of detection pipelines typically more sensitive than their low-latency  
886 counterparts, but comes at an additional computational cost and by definition cannot  
887 provide real-time alerts for astronomers.

888 The iDQ pipeline was also run in online and offline modes. As with CBC searches,  
889 the online configuration produced data available in near real-time to detection pipelines  
890 and data-quality experts. One detection pipeline, PyCBC Live [129], integrated the  
891 iDQ FAP timeseries into their search to reject candidate gravitational-wave signals  
892 caused by glitches. This implementation discarded all gravitational-wave candidates  
893 with coalescence times within one second of any time satisfying  $FAP(t) < 10^{-4}$ .

894 Offline iDQ differs from the low-latency version by having access to larger amounts  
895 of data when ranking and calibrating vetoes, allowing for more accurate estimation  
896 of their statistical properties. The log-likelihood timeseries produced by offline iDQ  
897 were used to construct data-quality flags. All of the times satisfying  $\log L(t) \geq 5$  were  
898 identified, and segments were constructed covering times from 0.25 s before to 0.25 s  
899 after each identified time. Data-quality flags were made by taking the union of all such  
900 segments. Different CBC searches may use these flags as they see fit. For example,  
901 the flags may be used as vetoes in the style of the Category 2 flags used in previous  
902 Observing runs, or they may be incorporated into a ranking statistic as in [130].

903 *4.2.2. Data quality for unmodelled transient searches* The coherent WaveBurst (cWB)  
904 pipeline [131] was the primary online search algorithm for unmodelled transients, or  
905 bursts, used in O4a. The cWB algorithm has several modes of operation which allow it  
906 to be applied to both short duration and long duration searches for GW signals from  
907 the entire sky, and searches for signals from binary black holes, Galactic core collapse  
908 supernovae or magnetar bursts or flares.

909 Times of poor data-quality were removed from the burst searches through Category  
910 1 and 2 flags as described above. All searches applied the same Category 1 flags as  
911 applied to the CBC searches, while Category 2 flags were developed by determining  
912 auxiliary data channels (those that monitor environmental or instrumental changes that  
913 are not sensitive to the effects of gravitational-waves) with high correlation to glitches  
914 that affect the burst searches. Category 2 flags are applied primarily to the offline burst  
915 searches. Similar to issues related to light intensity dips in O3, two Category 2 flags  
916 (one for the LHO and another for the LLO) were developed to exclude very loud glitches  
917 (usually with SNRs  $> 100$ ) [12]. These flags had deadtime percentages of order a tenth  
918 of a percent for each interferometer in O4a. There were 60 Hz glitches at LLO witnessed  
919 by ESD monitors which were used to develop an effective Category 2 flag specific to this  
920 observatory, with deadtime percentage of 0.069% during O4a.

921 *4.3. Data quality for persistent searches*

922 Persistent gravitational-wave signals are predicted to take a variety of forms.  
923 For example, rapidly-rotating non-axisymmetric neutron stars can emit nearly  
924 monochromatic gravitational-wave signals [132], a superposition of many gravitational-  
925 wave emitters can create a broadband stationary stochastic background [133], conditions  
926 in the early Universe may have generated a stochastic background signal [134], etc. The  
927 wide variety of possible signal models and our knowledge (or lack thereof) of waveform  
928 parameters motivates a similarly wide variety of analysis efforts [132, 135]. Nevertheless,  
929 these different search techniques may be served well by a relatively small number of  
930 data-quality products. Common data-quality products include information on which  
931 frequency bands are contaminated by narrowband noise lines, and cleaned strain data  
932 sets in which loud non-Gaussian transient noise has been removed. Different searches

933 take differing approaches towards handling non-stationary noise; CW searches tend  
934 to assign a lower weight to those time-frequency intervals of higher noise [136] while  
935 stochastic searches typically remove those periods from the analysis. Below we describe  
936 the data-quality products used for persistent searches in greater detail.

937 *4.3.1. Data quality for continuous wave searches*

938 *Self-gated  $h(t)$*  Although noise transients typically do not impact CW analyses, the  
939 cumulative effect of frequent and loud noise transients can degrade search sensitivity by  
940 effectively increasing the noise background, especially below  $\sim$ 500 Hz [12]. Removing  
941 these loud transient artifacts has proven useful in improving the sensitivity of broadband  
942 CW searches. In O4, we have employed a more sophisticated algorithm to identify  
943 and remove such artifacts, creating a new calibrated  $h(t)$  dataset useful for CW  
944 searches [137].

945 *Lists of narrow-band instrumental artifacts* Most CW searches depend on a catalog of  
946 known instrumental lines to veto spurious candidates or remove contaminated spectral  
947 bands from analysis. To produce the catalog, all lines visible in a high-resolution O4a-  
948 averaged spectrum (using Hann-windowed, 50% overlapping FFTs of 7200-second-long  
949 data segments) are listed and evaluated. Artifacts that are confirmed to be non-  
950 astrophysical are added to a curated list and made available for searches to use, as  
951 in [138]. Combs are always considered non-astrophysical because they do not align  
952 with a CW signal model. Other lines are considered non-astrophysical when their  
953 instrumental/environmental source is known. Artifacts that do not have identified  
954 non-astrophysical causes are placed in a separate curated list, as in [139]. Only the  
955 confirmed non-astrophysical list is used to veto outliers, whereas the unvetted list is  
956 used for investigation purposes.

957 *4.3.2. Data quality for stochastic searches*

958 *Non-stationarity cuts in stochastic searches.* Stochastic searches in LVK data are  
959 optimal under the assumption that the noise is stationary and Gaussian [133]. This  
960 is not the case in general, however, as introduced in section 1 and described throughout  
961 section 2. To mitigate these effects on stochastic analyses, we split our data into smaller  
962 segments, historically 192 s [140–142]. The data stationarity is enforced by removing  
963  $h(t)$  segments with a standard deviation that varies by more than a chosen threshold  
964 between adjacent segments [143].

965 *Auto-gating and stochastic DQ vetoes.* To mitigate the effect of glitches on frequency-  
966 domain non-stationarity cuts, a gating procedure is implemented to pre-process the  
967 data. In O4a, gating in stochastic searches is handled by the `pygwb` workflow [143] as  
968 described in [44] by multiplying the data with an inverse Planck-taper window. Periods

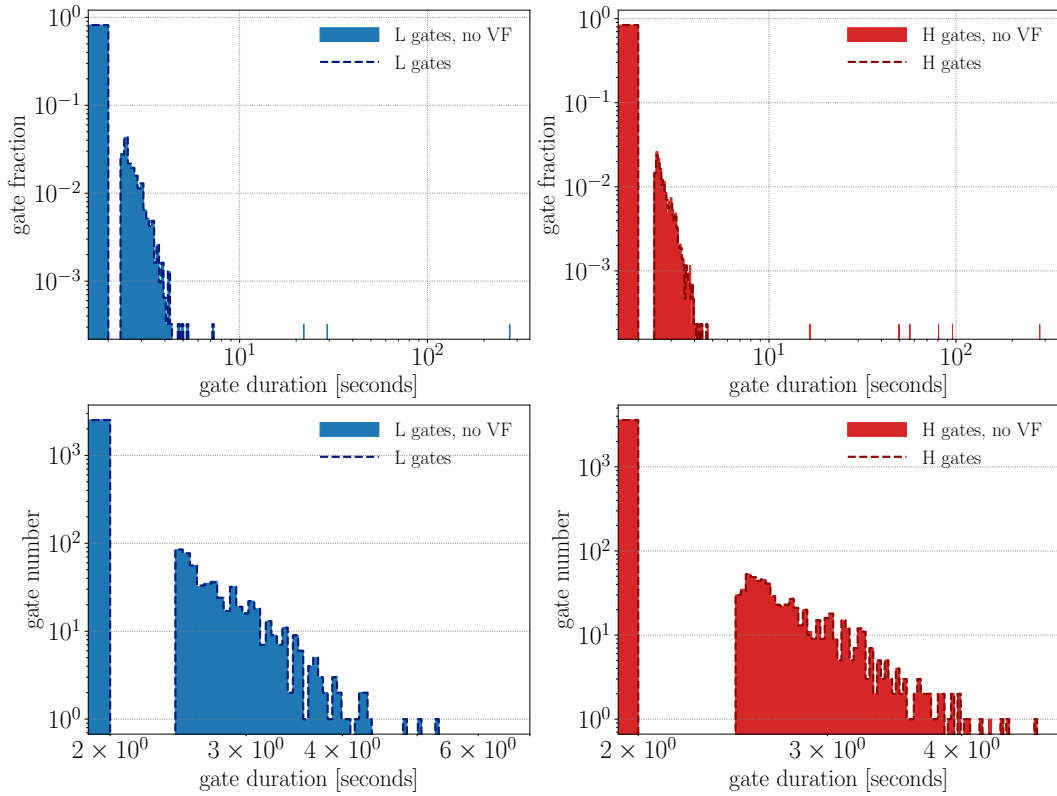


Figure 18: Effect on gate duration in stochastic data pre-processing for LLO (left-hand panels) and LHO (right-hand panels) when using the stochastic veto definer file (VF). The veto definer removes a small subset of times that correspond to the (few) long-duration gates. Gates are otherwise of duration  $< 10$  s;  $> 80\%$  have duration equal to the minimum gate duration (2 s), while the rest form a cluster of gates between [2.5, 4.5] s.

969 around samples in the whitened data with an absolute value above a chosen threshold  
 970 are marked for gating to remove the entirety of the glitch present in the data segment.  
 971 Occasionally, the gating method implemented in `pygwb` produces extended gates ( $\geq 20$  s)  
 972 that cover periods marked with Category 1 flags, as explained in section 4.1. This tool  
 973 helps monitoring the emergence of new Category 1 flagged periods.

974 In O4a, there are time segments marked with Category 1 flags unique to the  
 975 stochastic searches collected in a stochastic veto definer file (VF). These involve periods  
 976 when a violin mode was rung up and interfering with the stationarity of the data and  
 977 a specific instance when calibration lines were not being properly subtracted. The  
 978 stochastic isotropic search [44] was run with and without VF vetoed times to verify  
 979 that the VF correctly excludes data segments that trigger long gates. In figure 18,  
 980 we compare gate distributions between detectors. VF effectively removed long gates  
 981 in `pygwb` while maintaining overall bulk of the distribution. Of these gates, over 80%  
 982 match the minimum gate duration (2 s); others cluster between 2.5-4.5 s.

983 *Notch lists.* As described in section 2.1.5, we monitor the coherence between  $h(t)$   
984 channels at different sites, and between  $h(t)$  channel at one site and auxiliary channels at  
985 the same site. The coherence data between  $h(t)$  channels indicates the frequency bins  
986 that pass the coherence threshold as shown in figure 7. They are further examined  
987 for possible instrumental causes by spectral monitor tools that also keep track of  
988 auxiliary channels (Fscan, STAMP-PEM). Frequency bins containing lines known to have  
989 an instrumental origin are documented and removed from the analysis.

## 990 5. Summary and Future Prospects

991 There are multiple ways through which changes in environment impacts the GW strain  
992 data. DetChar group studies this interaction between the surrounding environment and  
993 the detector and develops tools to characterize and minimize the adverse impact on the  
994 GW data quality. In this paper, we summarize the work of the DetChar group between  
995 the end of the third Observing run and the end of the first half of the fourth Observing  
996 run. These efforts led to a factor of  $\sim 50$  reduction in the rate of daytime laser light  
997 scattering at LLO as detailed in 2.3.3, identification of the high-frequency magnetic  
998 noise coupling at LHO, identification of several persistent narrow-band noise features  
999 in LLO and LHO, a more comprehensive Event Validation and DQR framework and an  
1000 overall better understanding of the noise characteristics for astrophysical searches.

1001 As LIGO detectors become more sensitive, detector characterization will become  
1002 more challenging. Increased sensitivity translates to higher rate of events, but could  
1003 also lead to an increase in glitch rate. Our work entails not just glitch characterization  
1004 and reduction, but also validation of the data quality surrounding an event. Lower  
1005 detector noise across the band also implies higher sensitivity to persistent signals as well  
1006 as narrow-band, broad-band, and/or correlated terrestrial noise sources. Continuous  
1007 monitoring of the data quality, identification of potential noise couplings in the  
1008 detector, and improvement in our software tools are some of the prerequisites for timely  
1009 dissemination of robust, and accurate astrophysical results. This would, among other  
1010 things, require more person power, increased automation of tools such as DQR and  
1011 Event Validation, and stronger collaboration between instrument science and DetChar  
1012 group. These efforts will lead to more robust identification of weak astrophysical GW  
1013 signals in noisy LIGO data, and thus to a deeper probe of the GW sky.

1014 Data-quality products described in this paper from previous Observing runs have  
1015 been publicly released on the Gravitational Wave Open Science Center (GWOSC)  
1016 webpage [||](#), and when the O4a data are publicly released, data-quality products will  
1017 be released alongside [144].

## 1018 Acknowledgments

1019 We would like to thank Christopher Berry, Jess McIver and Alan Weinstein for their

many helpful comments and suggestions. This material is based upon work supported by NSF's LIGO Laboratory which is a major facility fully funded by the National Science Foundation. LIGO was constructed by the California Institute of Technology and Massachusetts Institute of Technology with funding from the National Science Foundation and operates under Cooperative Agreement PHY-1764464. Advanced LIGO was built under grant No. PHY-0823459. This work uses the LIGO computing clusters and data from the Advanced LIGO detectors. This document has been assigned LIGO-number LIGO-P2400320.

1028 **References**

- [1] Aasi J *et al.* (LIGO Scientific) 2015 *Class. Quant. Grav.* **32** 074001 (*Preprint* [1411.4547](https://arxiv.org/abs/1411.4547))
- [2] Acernese F *et al.* (Virgo) 2015 *Class. Quant. Grav.* **32** 024001 (*Preprint* [1408.3978](https://arxiv.org/abs/1408.3978))
- [3] Abbott B P *et al.* (LIGO Scientific Collaboration and Virgo Collaboration) 2016 *Phys. Rev. Lett.* **116**(6) 061102 <https://link.aps.org/doi/10.1103/PhysRevLett.116.061102>
- [4] Abbott B P *et al.* (LIGO Scientific, Virgo) 2019 *Phys. Rev. X* **9** 031040 (*Preprint* [1811.12907](https://arxiv.org/abs/1811.12907))
- [5] Abbott R *et al.* (LIGO Scientific, Virgo) 2024 *Phys. Rev. D* **109** 022001 (*Preprint* [2108.01045](https://arxiv.org/abs/2108.01045))
- [6] Abbott R *et al.* (KAGRA, Virgo, LIGO Scientific) 2023 *Phys. Rev. X* **13** 041039 (*Preprint* [2111.03606](https://arxiv.org/abs/2111.03606))
- [7] Abbott B P *et al.* (LIGO Scientific, Virgo) 2017 *Phys. Rev. Lett.* **119** 161101 (*Preprint* [1710.05832](https://arxiv.org/abs/1710.05832))
- [8] Ganapathy D *et al.* (LIGO O4 Detector) 2023 *Phys. Rev. X* **13** 041021
- [9] Abac A G *et al.* (LIGO Scientific, Virgo,, KAGRA, VIRGO) 2024 *Astrophys. J. Lett.* **970** L34 (*Preprint* [2404.04248](https://arxiv.org/abs/2404.04248))
- [10] Davis D *et al.* 2021 *Class. Quant. Grav.* **38** 135014 (*Preprint* [2101.11673](https://arxiv.org/abs/2101.11673))
- [11] Macleod D, Goetz E, Ota I, Isi M *et al.* 2024 gwpy/gwsumm: 2.2.6 <https://doi.org/10.5281/zenodo.10999143>
- [12] Davis D *et al.* (LIGO) 2021 *Class. Quant. Grav.* **38** 135014 (*Preprint* [2101.11673](https://arxiv.org/abs/2101.11673))
- [13] Abbott B P *et al.* (LIGO Scientific, Virgo) 2020 *Class. Quant. Grav.* **37** 055002 (*Preprint* [1908.11170](https://arxiv.org/abs/1908.11170))
- [14] Zevin M *et al.* 2017 *Class. Quant. Grav.* **34** 064003 (*Preprint* [1611.04596](https://arxiv.org/abs/1611.04596))
- [15] Glanzer J, Banagiri S, Coughlin S B, Soni S *et al.* 2023 *Classical and Quantum Gravity* **40** 065004 [http://dx.doi.org/10.1088/1361-6382/acb633](https://dx.doi.org/10.1088/1361-6382/acb633)
- [16] Covas P B, Effler A, Goetz E, Meyers P M *et al.* (LSC Instrument Authors) 2018 *Phys. Rev. D* **97**(8) 082002 <https://link.aps.org/doi/10.1103/PhysRevD.97.082002>
- [17] Soni S *et al.* (LIGO) 2020 *Class. Quant. Grav.* **38** 025016 (*Preprint* [2007.14876](https://arxiv.org/abs/2007.14876))
- [18] Soni S, Glanzer J, Effler A, Frolov V *et al.* 2024 *Class. Quant. Grav.* **41** 135015 (*Preprint* [2311.05730](https://arxiv.org/abs/2311.05730))
- [19] Berger B K *et al.* 2023 *Appl. Phys. Lett.* **122** 184101
- [20] Nguyen P *et al.* (AdvLIGO) 2021 *Class. Quant. Grav.* **38** 145001 (*Preprint* [2101.09935](https://arxiv.org/abs/2101.09935))
- [21] Karki S *et al.* 2016 *Rev. Sci. Instrum.* **87** 114503 (*Preprint* [1608.05055](https://arxiv.org/abs/1608.05055))

- [22] Biwer C *et al.* 2017 *Phys. Rev. D* **95** 062002 (*Preprint* [1612.07864](https://arxiv.org/abs/1612.07864))
- [23] Robinet F, Arnaud N, Leroy N, Lundgren A *et al.* 2020 *SoftwareX* **12** 100620 (*Preprint* [2007.11374](https://arxiv.org/abs/2007.11374))
- [24] Soni S *et al.* 2021 *Class. Quant. Grav.* **38** 195016 (*Preprint* [2103.12104](https://arxiv.org/abs/2103.12104))
- [25] Zevin M *et al.* 2024 *Eur. Phys. J. Plus* **139** 100 (*Preprint* [2308.15530](https://arxiv.org/abs/2308.15530))
- [26] Brown J C 1991 *The Journal of the Acoustical Society of America* **89** 425–34
- [27] Chatterji S, Blackburn L, Martin G and Katsavounidis E 2004 *Classical and Quantum Gravity* **21** S1809
- [28] Smith J R, Abbott T, Hirose E, Leroy N *et al.* 2011 *Class. Quant. Grav.* **28** 235005 (*Preprint* [1107.2948](https://arxiv.org/abs/1107.2948))
- [29] Ramirez K *Lockloss at 05:14 UTC due to an EQ* <https://alog.ligo-la.caltech.edu/aLOG/index.php?callRep=68196>
- [30] Cessaro R K 1994 *Bulletin of the Seismological Society of America* **84** 142–8 <https://doi.org/10.1785/BSSA0840010142>
- [31] Ottaway D J, Fritschel P and Waldman S J 2012 *Optics Express* **20** 8329
- [32] Accadia T *et al.* 2010 *Class. Quant. Grav.* **27** 194011
- [33] Ottaway D J, Fritschel P and Waldman S J 2012 *Opt. Express* **20** 8329–36 <https://opg.optica.org/oe/abstract.cfm?URI=oe-20-8-8329>
- [34] Soni S and Effler A 2024 *Microseismic induced scatter at LLO in O4a* <https://dcc.ligo.org/LIGO-G2400653>
- [35] Schofield R *Cryo-baffle barrel may be the dominant source of ~1 Hz vibration coupling at EY* <https://alog.ligo-wa.caltech.edu/aLOG/index.php?callRep=55927>
- [36] Fritschel P *Layout of Stray Light Control Baffles* [D1600493](#)
- [37] Schofield R *Does vibration coupling tend to increase with main laser power? Coupling dropped at PSL by roughly two and at EX by three when power was dropped from 75W to 60W* <https://alog.ligo-wa.caltech.edu/aLOG/index.php?callRep=70808>
- [38] Effler A *EX Cryobaffle damped* <https://alog.ligo-la.caltech.edu/aLOG/index.php?callRep=69280>
- [39] Schofield R *et al.* *Through-viewport damping of EX Cryobaffle reduced Q from 400 to 20, which should reduce scattering shelf cut-off proportionally* <https://alog.ligo-wa.caltech.edu/aLOG/index.php?callRep=75553>
- [40] Essick R, Mo G and Katsavounidis E 2021 *Phys. Rev. D* **103** 042003 (*Preprint* [2011.13787](https://arxiv.org/abs/2011.13787))
- [41] Goetz E, Neunzert A and Suyamprakasam S 2024 Fscan <https://doi.org/10.5281/zenodo.10966714>

- [42] Meyers P M 2018 *Cross-correlation searches for persistent gravitational waves with Advanced LIGO and noise studies for current and future ground-based gravitational-wave detectors* Ph.D. thesis Minnesota U.
- [43] Hernandez G and E T 2023 *Stochmon: A LIGO Data Analysis Tool* Tech. Rep. T1400205 LSC <https://dcc.ligo.org/LIGO-T1400205/public>
- [44] Renzini A I, Romero-Rodríguez A, Talbot C, Lalleman M *et al.* 2023 *The Astrophysical Journal* **952** 25 <http://dx.doi.org/10.3847/1538-4357/acd775>
- [45] Kissel J *Low-frequency Thermalization lines are OFF as of 2023-08-09 16:40 UTC* <https://alog.ligo-wa.caltech.edu/aLOG/index.php?callRep=72096>
- [46] Kandhasamy S *DuoTone line frequencies in DARM spectra* <https://alog.ligo-la.caltech.edu/aLOG/index.php?callRep=64525>
- [47] Janssens K, Martinovic K, Christensen N, Meyers P M and Sakellariadou M 2021 *Phys. Rev. D* **104** 122006 [Erratum: Phys.Rev.D 105, 109904 (2022)] (*Preprint* 2110.14730)
- [48] Schofield R and Dwyer S *Update on grounding noise studies* <https://alog.ligo-wa.caltech.edu/aLOG/index.php?callRep=67075>
- [49] Schofield R *et al.* 95 Hz peak reduced in ESD power supply monitor; DARM not yet checked <https://alog.ligo-wa.caltech.edu/aLOG/index.php?callRep=65907>
- [50] Schofield R *et al.* EX ground noise coupling further reduced by new ground straps, and coupling is proportional to bias <https://alog.ligo-wa.caltech.edu/aLOG/index.php?callRep=66469>
- [51] Schofield R *ETMX bias that minimizes grounding noise coupling hasnt changed much since January, and PEM injections at 60W* <https://alog.ligo-wa.caltech.edu/aLOG/index.php?callRep=72118>
- [52] Effler A *et al.* *PEM Injections Status* <https://alog.ligo-la.caltech.edu/aLOG/index.php?callRep=64609>
- [53] Effler A and Ferreira T *Disappearance of the 35.7Hz line on the DARM channel* <https://alog.ligo-la.caltech.edu/aLOG/index.php?callRep=67581>
- [54] Vajente G *DARM bicoherence: evidence of non-stationary noise 10-50 Hz* <https://alog.ligo-wa.caltech.edu/aLOG/index.php?callRep=71005>
- [55] Vajente G *DARM noise 20-40 Hz correlated with 2.6 Hz peak* <https://alog.ligo-wa.caltech.edu/aLOG/index.php?callRep=71092>
- [56] Vajente G *Low frequency noise improved with new CHARD Y controller and reduced TM damping* <https://alog.ligo-wa.caltech.edu/aLOG/index.php?callRep=71927>
- [57] Compton C *Next lock at 60W input power.* <https://alog.ligo-wa.caltech.edu/aLOG/index.php?callRep=70648>

- [58] Short R, Glanzer J, Helmling-Cornell A, Effler A and Schofield R *PEM injections successfully completed - will inform HVAC experiments* <https://alog.ligo-wa.caltech.edu/aLOG/index.php?callRep=69745>
- [59] Effler A, Schofield R M S, Frolov V V, González G *et al.* 2015 *Class. Quant. Grav.* **32** 035017 (*Preprint* 1409.5160)
- [60] Thorne K S 1969 *ApJ* **158** 1
- [61] Ho W C G, Jones D I, Andersson N and Espinoza C M 2020 *Phys. Rev. D* **101** 103009 (*Preprint* 2003.12082)
- [62] Ball M, Frey R and Merfeld K 2024 *Monthly Notices of the Royal Astronomical Society* stae1987 (*Preprint* 2310.15315)
- [63] Helmling-Cornell A F, Nguyen P, Schofield R M S and Frey R 2024 *Classical and Quantum Gravity* **41** 145003 (*Preprint* 2312.00735)
- [64] Braginsky V B, Ryazhskaya O G and Vyatchanin S P 2006 *Phys. Lett. A* **350** 1–4 (*Preprint* gr-qc/0509058)
- [65] Yamamoto K, Hayakawa H, Okada A, Uchiyama T *et al.* 2008 *Phys. Rev. D* **78** 022004 (*Preprint* 0805.2387)
- [66] Mannix B and Frey R *Search for Cosmic Ray Induced Transient Noise at LIGO Hanford* <https://dcc.ligo.org/LIGO-T2400290/public>
- [67] Guidry T, Otterman E, McCarthy R and Schofield R *Sitewide HVAC shutdown increases range to about 169 Mpc* <https://alog.ligo-wa.caltech.edu/aLOG/index.php?callRep=73941>
- [68] Schofield R *CER ACs and main HVAC likely couple to DARM in input arm, possibly through MCA2 baffle* <https://alog.ligo-wa.caltech.edu/aLOG/index.php?callRep=74175>
- [69] Schofield R *Confirmation from laser vibrometry and beating shakers: the MC baffle by HAM3 has been producing noise in DARM and the one by HAM2 produces noise when 18 Hz vibration is increased by about 5; also, suggestions for mitigation during the January break* <https://alog.ligo-wa.caltech.edu/aLOG/index.php?callRep=74772>
- [70] Schofield R *et al.* *Summary of scattering mitigation in the input MC tube with before/after pictures* <https://alog.ligo-wa.caltech.edu/aLOG/index.php?callRep=75726>
- [71] Schofield R *Evaluation of stray light work done during the break: desired reductions in vibration coupling attained for EX cryobaffle, and for input arm - after adjustment of ITMY CP yaw* <https://alog.ligo-wa.caltech.edu/aLOG/index.php?callRep=76969>
- [72] Goetz E *OM2 heater suspected culprit for 1.6611 Hz comb in h(t)* <https://alog.ligo-wa.caltech.edu/aLOG/index.php?callRep=71801>
- [73] Kawabe K, Clara F and Mera F *OM2 thermistor sensor voltage supplies are oscillating* <https://alog.ligo-wa.caltech.edu/aLOG/index.php?callRep=73886>

- [74] Barsotti L, Evans M and Fritschel P 2010 *Classical and Quantum Gravity* **27** 084026 <https://dx.doi.org/10.1088/0264-9381/27/8/084026>
- [75] Neunzert A *Very weak 0.996785 Hz comb present for a few months* <https://alog.ligo-wa.caltech.edu/aLOG/index.php?callRep=74614>
- [76] Compton C *ITM HWS Camera Sync Frequencies Adjusted to 7Hz for DARM Comb Search* <https://alog.ligo-wa.caltech.edu/aLOG/index.php?callRep=74617>
- [77] Compton C, Clara F, Sanchez L and Baxi P *Changed Wiring in HWS Camera External Power Supply - Have proposed coupling of combs!* <https://alog.ligo-wa.caltech.edu/aLOG/index.php?callRep=75876>
- [78] Glanzer J, Soni S, Spoon J, Effler A and González G 2023 *Class. Quant. Grav.* **40** 195015 (*Preprint* 2304.07477)
- [79] Tibshirani R 1996 *Journal of the Royal Statistical Society. Series B (Methodological)* **58** 267–88 <http://www.jstor.org/stable/2346178>
- [80] Boslaugh S and Watters P 2009 *Statistics in a nutshell: A desktop quick reference* (O'Reilly Media, Inc.)
- [81] Traylor G *Logging near the cornerstation* <https://alog.ligo-la.caltech.edu/aLOG/index.php?callRep=65149>
- [82] Traylor G *Preparations for logging on LIGO Rd* <https://alog.ligo-la.caltech.edu/aLOG/index.php?callRep=65404>
- [83] M Smith V S 2011 *Arm Cavity Baffle Final Design (SLC)* T1000747
- [84] Wen S *et al.* 2014 *Class. Quant. Grav.* **31** 235001 (*Preprint* 1309.5685)
- [85] Effler A 2022 aLIGO LLO Logbook 60927
- [86] Soni S *ETMY HEPI sweep Injections* <https://alog.ligo-la.caltech.edu/aLOG/index.php?callRep=63569>
- [87] Soni S *Comment: ETMY HEPI sweep Injections* <https://alog.ligo-la.caltech.edu/aLOG/index.php?callRep=63699>
- [88] Soni S *Cornerstation logging noise comparison with O3* <https://alog.ligo-la.caltech.edu/aLOG/index.php?callRep=65494>
- [89] Glanzer J *Investigating fluctuating BNS range on May 22nd and May 24th* <https://alog.ligo-la.caltech.edu/aLOG/index.php?callRep=65146>
- [90] Glanzer J *Continuation of BNS fluctuation investigations* <https://alog.ligo-la.caltech.edu/aLOG/index.php?callRep=65497>
- [91] Glanzer J *Investigating HVAC shutdown and BNS oscillations* <https://alog.ligo-la.caltech.edu/aLOG/index.php?callRep=68041>
- [92] Glanzer J *Comment to: Noise in DARM due to ground motion peaks at 15 Hz and its multiples near EX* <https://alog.ligo-la.caltech.edu/aLOG/index.php?callRep=70525>

- [93] Walker M, Agnew A F, Bidler J, Lundgren A *et al.* 2018 *Class. Quant. Grav.* **35** 225002 (*Preprint* [1807.02592](https://arxiv.org/abs/1807.02592))
- [94] Soni S *BNS range oscillations on Dec 13 and Dec 14* <https://alog.ligo-la.caltech.edu/aLOG/index.php?callRep=69034>
- [95] Effler A and Frolov V *Quad blades show drift in temperature control at all stations* <https://alog.ligo-la.caltech.edu/aLOG/index.php?callRep=69020>
- [96] Strong M and Effler A *84 hz in DARM likely from Y arm exhaust fan near corner station* <https://alog.ligo-la.caltech.edu/aLOG/index.php?callRep=63964>
- [97] Effler A *End Station Acoustic Injections - 83 Hz likely from EY* <https://alog.ligo-la.caltech.edu/aLOG/index.php?callRep=63399>
- [98] Effler A *84 Hz in DARM modulated by EY Y2J fan specifically* <https://alog.ligo-la.caltech.edu/aLOG/index.php?callRep=64265>
- [99] Cornish N J, Littenberg T B, Bécsy B, Chatzioannou K *et al.* 2021 *Phys. Rev. D* **103** 044006 (*Preprint* [2011.09494](https://arxiv.org/abs/2011.09494))
- [100] Davis D 2020 *LIGO Event Validation for O3* Tech. Rep. G2000395 LSC <https://dcc.ligo.org/LIGO-G2000395>
- [101] Abbott R *et al.* (LIGO Scientific, Virgo, KAGRA) 2021 *Preprint* [2111.03606](https://arxiv.org/abs/2111.03606)
- [102] Abbott R *et al.* (LIGO Scientific, Virgo) 2021 *Phys. Rev. X* **11** 021053 (*Preprint* [2010.14527](https://arxiv.org/abs/2010.14527))
- [103] Acernese F *et al.* (Virgo) 2023 *Class. Quant. Grav.* **40** 185006 (*Preprint* [2210.15633](https://arxiv.org/abs/2210.15633))
- [104] Davis D, Yarbough Z, Areeda J *et al.* 2024 In Preparation
- [105] Acernese F *et al.* (Virgo) 2023 *Class. Quant. Grav.* **40** 185005 (*Preprint* [2210.15634](https://arxiv.org/abs/2210.15634))
- [106] Essick R, Godwin P, Hanna C, Blackburn L and Katsavounidis E 2020 *Preprint* [2005.12761](https://arxiv.org/abs/2005.12761)
- [107] Vazsonyi L and Davis D 2023 *Class. Quant. Grav.* **40** 035008 (*Preprint* [2208.12338](https://arxiv.org/abs/2208.12338))
- [108] Chatterji S, Blackburn L, Martin G and Katsavounidis E 2004 *Class. Quant. Grav.* **21** S1809–18 (*Preprint* [0412119](https://arxiv.org/abs/0412119))
- [109] Alvarez-Lopez S, Liyanage A, Ding J, Ng R and McIver J 2024 *Class. Quant. Grav.* **41** 085007 (*Preprint* [2304.09977](https://arxiv.org/abs/2304.09977))
- [110] Mozzon S, Nuttall L K, Lundgren A, Dent T *et al.* 2020 *Class. Quant. Grav.* **37** 215014 (*Preprint* [2002.09407](https://arxiv.org/abs/2002.09407))
- [111] Doleva P, Walker M, Team L *et al.* 2022 *Analysis of the Average Glitch Rate Around a Gravitational Wave Event Candidate APS April Meeting Abstracts* vol 2022 pp F01–064
- [112] Davis D, Littenberg T B, Romero-Shaw I M, Millhouse M *et al.* 2022 *Class. Quant. Grav.* **39** 245013 (*Preprint* [2207.03429](https://arxiv.org/abs/2207.03429))

- [113] Cornish N J and Littenberg T B 2015 *Class. Quant. Grav.* **32** 135012 (*Preprint* [1410.3835](https://arxiv.org/abs/1410.3835))
- [114] Ashton G *et al.* 2024 CBCFlow <https://cbc.docs.ligo.org/projects/cbcflow/index.html>
- [115] LIGO Scientific Collaboration, Virgo Collaboration and KAGRA Collaboration 2023 *General Coordinates Network* **35000** 1 <https://gcn.nasa.gov/circulars/35000>
- [116] LIGO Scientific Collaboration, Virgo Collaboration and KAGRA Collaboration 2023 *General Coordinates Network* **34911** 1 <https://gcn.nasa.gov/circulars/34911>
- [117] LIGO Scientific Collaboration, Virgo Collaboration and KAGRA Collaboration 2023 *General Coordinates Network* **34728** 1 <https://gcn.nasa.gov/circulars/34728>
- [118] LIGO Scientific Collaboration, VIRGO Collaboration and Kagra Collaboration 2023 *General Coordinates Network* **34599** 1 <https://gcn.nasa.gov/circulars/34599>
- [119] LIGO Scientific Collaboration, Virgo Collaboration and KAGRA Collaboration 2023 *General Coordinates Network* **34378** 1 <https://gcn.nasa.gov/circulars/34378>
- [120] LIGO Scientific Collaboration, Virgo Collaboration and KAGRA Collaboration 2023 *General Coordinates Network* **34367** 1 <https://gcn.nasa.gov/circulars/34367>
- [121] LIGO Scientific Collaboration, Virgo Collaboration and KAGRA Collaboration 2023 *General Coordinates Network* **34219** 1 <https://gcn.nasa.gov/circulars/34219>
- [122] LIGO Scientific Collaboration, Virgo Collaboration and KAGRA Collaboration 2023 *General Coordinates Network* **34206** 1 <https://gcn.nasa.gov/circulars/34206>
- [123] LIGO Scientific Collaboration, Virgo Collaboration and KAGRA Collaboration 2023 *General Coordinates Network* **34172** 1 <https://gcn.nasa.gov/circulars/34172>
- [124] LIGO Scientific Collaboration, Virgo Collaboration and KAGRA Collaboration 2023 *General Coordinates Network* **34065** 1 <https://gcn.nasa.gov/circulars/34065>
- [125] LIGO Scientific Collaboration, Virgo Collaboration and KAGRA Collaboration 2023 *General Coordinates Network* **33871** 1 <https://gcn.nasa.gov/circulars/33871>
- [126] Evans M, Gras S, Fritschel P, Miller J *et al.* 2015 *Phys. Rev. Lett.* **114**(16) 161102 <https://link.aps.org/doi/10.1103/PhysRevLett.114.161102>

- [1297] [127] Abbott B P *et al.* (LIGO Scientific Collaboration and Virgo Collaboration) 2016 *Phys. Rev. Lett.* **116**(13) 131103 <https://link.aps.org/doi/10.1103/PhysRevLett.116.131103>
- [1298]
- [1299]
- [1300] [128] Essick R, Blackburn L and Katsavounidis E 2013 *Class. Quant. Grav.* **30** 155010 (*Preprint* [1303.7159](https://arxiv.org/abs/1303.7159))
- [1301]
- [1302] [129] Dal Canton T, Nitz A H, Gadre B, Cabourn Davies G S *et al.* 2021 *Astrophys. J.* **923** 254 (*Preprint* [2008.07494](https://arxiv.org/abs/2008.07494))
- [1303]
- [1304] [130] Davis D, Trevor M, Mozzon S and Nuttall L K 2022 *Phys. Rev. D* **106** 102006 (*Preprint* [2204.03091](https://arxiv.org/abs/2204.03091))
- [1305]
- [1306] [131] Szczepańczyk M J, Salemi F, Bini S, Mishra T *et al.* 2023 *Phys. Rev. D* **107**(6) 062002 <https://link.aps.org/doi/10.1103/PhysRevD.107.062002>
- [1307]
- [1308] [132] Wette K 2023 *Astroparticle Physics* **153** 102880 <https://www.sciencedirect.com/science/article/pii/S092765052300066X>
- [1309]
- [1310] [133] Renzini A I, Goncharov B, Jenkins A C and Meyers P M 2022 *Galaxies* **10** <https://www.mdpi.com/2075-4434/10/1/34>
- [1311]
- [1312] [134] Caprini C and Figueroa D G 2018 *Class. Quant. Grav.* **35** 163001 (*Preprint* [1801.04268](https://arxiv.org/abs/1801.04268))
- [1313]
- [1314] [135] Romano J D and Cornish N J 2017 *Living Rev. Rel.* **20** 2 (*Preprint* [1608.06889](https://arxiv.org/abs/1608.06889))
- [1315] [136] Riles K 2023 *Living Reviews in Relativity* **26**
- [1316] [137] Davis D, Neunzert A *et al.* 2024 *Self-gating of O4a h(t) for use in continuous-wave searches* Tech. Rep. T2400003 LSC <https://dcc.ligo.org/LIGO-T2400003>
- [1317]
- [1318] [138] Goetz E *et al.* 2021 *O3 lines and combs in found in self-gated C01 data* Tech. Rep. T2100200 LSC <https://dcc.ligo.org/LIGO-T2100200/public>
- [1319]
- [1320] [139] Goetz E *et al.* 2021 *Unidentified O3 lines found in self-gated C01 data* Tech. Rep. T2100201 LSC <https://dcc.ligo.org/LIGO-T2100201/public>
- [1321]
- [1322] [140] Abbott B P *et al.* (LIGO Scientific, Virgo) 2017 *Phys. Rev. Lett.* **118** 121101 [Erratum: Phys.Rev.Lett. 119, 029901 (2017)] (*Preprint* [1612.02029](https://arxiv.org/abs/1612.02029))
- [1323]
- [1324] [141] Abbott B P *et al.* (LIGO Scientific, Virgo) 2019 *Phys. Rev. D* **100** 061101 (*Preprint* [1903.02886](https://arxiv.org/abs/1903.02886))
- [1325]
- [1326] [142] Abbott R *et al.* (KAGRA, Virgo, LIGO Scientific) 2021 *Phys. Rev. D* **104** 022004 (*Preprint* [2101.12130](https://arxiv.org/abs/2101.12130))
- [1327]
- [1328] [143] Renzini A I, Romero-Rodriguez A, Talbot C, Lalleman M *et al.* 2024 *Journal of Open Source Software* **9** 5454 <https://doi.org/10.21105/joss.05454>
- [1329]
- [1330] [144] Abbott R *et al.* (KAGRA, VIRGO, LIGO Scientific) 2023 *Astrophys. J. Suppl.* **267** 29 (*Preprint* [2302.03676](https://arxiv.org/abs/2302.03676))
- [1331]